Integrated stratigraphy and paleoceanographic evolution of the pre-evaporitic phase of the Messinian salinity crisis in the Eastern Mediterranean as recorded in the Tokhni section (Cyprus island)

Gennari Rocco[a,b,c], Lozar Francesca[c], Turco Elena[a], Dela Pierre Francesco[c], Manzi Vinicio[a,b], Natalicchio Marcello[c,d], Lugli Stefano[e], Roveri Marco[a,b], Schreiber B. Charlotte[f], Taviani Marco[g,h,i]

[a] Physics and Earth Science Department, University of Parma, Parco Area delle Scienze, 157/A 43124 Parma, Italy. E-mails: rocco.gennari@gmail.com (corresponding author), elena.turco@unipr.it, vinicio.manzi@unipr.it, marco.roveri@unipr.it

[b] ALP, Alpine Laboratory of Palaeomagnetism, Via G.U. Luigi Massa, 6, 12016 Peveragno, CN, Italy.

[c] Earth Science Department, University of Turin, Via T. Valperga Caruso, 35, 10125, Torino, Italy. E-mails: francesca.lozar@unito.it, francesco.delapierre@unito.it, marcello.natalicchio@unito.it

[d] Institute of Geology, University of Hamburg, Bundesstraße 55, 20146 Hamburg, Germany

[e] Chemical and Geological Department, University of Modena and Reggio Emilia, Campus Scientifico, Via G. Campi, 183, 41125 Modena, Italy. E-mail: stefano.lugli@unimore.it

[f] Department of Earth and Space Sciences, University of Washington, Johnson Hall Rm-070, 4000 15th Avenue NE, Seattle, WA 98195-1310, USA. E-mail: geologo1@u.washington.edu

[g] ISMAR-CNR, Via Gobetti 101, 40129 Bologna, Italy. E-mail: marco.taviani@bo.ismar.cnr.it

[h] Biology Department, Woods Hole Oceanographic Institution, 266 Woods Hole Rd, Woods Hole, Ma. 02543, USA.

[i] Stazione Zoologica Anton Dohrn, Villa Comunale, 80121 Napoli, Italy.

Abstract

An integrated micropaleontologic, magnetostratigraphic and cyclostratigraphic investigation of the Tokhni composite section (Southern Cyprus Island, Eastern Mediterranean) refines the previously published age model and paleoenvironmental interpretation particularly concerning its uppermost pre-Messinian Salinity Crisis interval

(pre-MSC), between 6.46 and 5.97 Ma. This section is characterized by a precession-paced alternation of red shales and limestones, which correlate with insolation maxima and minima on the basis of their $\partial^{18}O$ signatures and calcareous nannofossil assemblages. The planktonic foraminifer and magnetostratigraphic events permit the tuning of the sedimentary cycles to the 65°N summer insolation curve and to the Mediterranean pre-evaporitic reference sections.

The upper bathyal sedimentary succession of the Tokhni composite section records paleoceanographic changes at 6.4 and 6.1 Ma, indicating increasingly stressed conditions both at the sea floor and in the water column. Compared to the Western Mediterranean pre-MSC successions, we observe less severe sea floor anoxic conditions at times of insolation maxima and higher salinity surface and bottom waters at times of insolation minima. Moreover, from 6.1 Ma to the MSC onset we observe a progressively increase of continental-derived waters, which was likely caused by a tectonic pulse.

The MSC onset at 5.97 Ma is marked by the deposition of clastic carbonates rather than primary evaporitic facies and is approximated by the last recovery of foraminifera, the abundance peaks of *Helicosphaera carteri* and *Umbilicosphaera rotula* and the decrease of the $^{87/86}Sr$. The MSC onset is recorded two cycles below the Messinian Erosional Surface (MES, 5.60 Ma) and the overlying clastic evaporites, suggesting a hiatus of approximately 350 kyr.

Keywords: Eastern Mediterranean, Messinian, calcareous nannofossils, foraminifera, integrated stratigraphy, paleoenvironment.

1. Introduction

The pre-evaporitic phase of the Messinian salinity crisis (MSC) was characterized by marked paleoceanographic changes culminating in the deposition of huge volume of

evaporites in the shallow and deep/intermediate settings of the Mediterranean basin during stage 1 (from 5.971 Ma; Manzi et al. 2013) and stage 2 (from 5.60 Ma; Roveri et al. 2009), respectively. The major steps of this paleoceanographic evolution occurred at 7.16, 6.7, 6.4 - 6.29 and 6.1 - 6.0 Ma (see Kouwenhoven et al. 2006, with references therein). Each of these steps was conductive to increasingly stressing conditions both at the sea floor and in the water column, as documented by the progressive increase of oligotypic calcareous plankton and benthic foraminifer assemblages. The first two steps were related to the tectonic narrowing and/or closure of the Atlantic connections in the Rifian corridors (Krijgsman et al. 1999a and b, Krijgsman and Langereis 2000), which caused the slowing or stopping of the Mediterranean deep circulation. However, Blanc-Valleron et al. (2002) noted that these paleoceanographic steps roughly follow the 400 kyr eccentricity cycle, and Kouwenhoven et al. (2006) also suggested a relation between the increasing restriction of the deep circulation and this orbital parameter. In addition, the restricted connections with the Atlantic from 7.16 Ma increased the sensitivity of the Mediterranean basin to record the precession-controlled climatic changes resulting in a more regular formation of sapropels at times of precession minima (Sierro et al. 2003).

In the deep- and intermediate-water successions, such as at Monte del Casino (northern Apennines, Italy) and Pissouri (southern Cyprus) sections, respectively (Kouwenhoven et al. 2003; Kouwenhoven et al. 2006), the step at 7.16 Ma was characterized by the disappearance of oxyphilic benthic foraminifera and the increase of taxa tolerating low oxygen levels and raised salinity (Van der Zwaan 1982, Kouwenhoven et al. 1999). As seen in the Gibliscemi-Falconara sections (Sicily), the central Mediterranean was more severely affected by the reduced deep-water circulation, marked by a temporarily disappearance of benthic foraminifera (Kouwenhoven et al. 2003). Moreover, diatomite beds started to deposit in the Mediterranean between 7.16 and 6.7 Ma (Pestrea et al. 2002), indicating a significant availability of silica at times of enhanced eutrophication,

likely connected to upwelling episodes during insolation minima (Sierro et al. 2003, Flores et al. 2005).

Beginning at 6.7 Ma (second step), not only the benthic foraminifera show an abundance increase of stress tolerant taxa (indicating low oxygen and/or raised salinity bottom conditions) and are absent in sapropel (Sierro et al. 2003, Kouwenhoven et al. 2006), but also the calcareous plankton assemblages are characterized by reduced diversity and abundance (Sierro et al. 2003). Moreover, an increased response to the insolation fluctuations is highlighted by the dominance of cold/eutrophic calcareous plankton taxa at times of insolation minima and warm/oligotrophic taxa at times of insolation maxima (Blanc-Valleron et al. 2002, Sierro et al. 2003, Flores et al. 2005). It is worth noting that changes in calcareous plankton assemblages from 6.7 Ma equally affected both deep and shallow successions.

From 6.4 Ma the Plankton/Benthos ratio shows abrupt fluctuations, with values ranging from 100% to near 0%, indicating the occurrence of a-benthic foraminiferal layers due to anoxic conditions during insolation maxima and of strongly reduced/a-planktonic layers (insolation minima) (Sierro et al. 2003). In the superficial waters, the presence of oligotypic assemblages dominated by *Turborotalia quinqueloba* and *T. multiloba* (up to 80%) during insolation minima are usually related to increased salinity corresponding to very arid climatic phases (Sierro et al. 2003, Kouwenhoven et al. 2006).

The final step at 6.1 - 6.0 Ma certifies the gradual final decrease of calcareous microfossils, whose disappearance approximates the MSC onset at 5.971 Ma (Manzi et al. 2007, Lozar et al. 2010, Manzi et al. 2011, Manzi et al. 2013).

The eastern Mediterranean pre-evaporitic (pre-MSC) micropaleontologic record has been mainly studied onshore of Cyprus and Crete (Van der Zwaan, 1982, Triantaphyllou et al. 1999, Kouwenhoven et al. 2006, Drinia et al. 2007, Orszag-Sperber et al. 2009). On the southern part of the Cyprus Island, an integrated stratigraphy was obtained for the Tokhni

and Pissouri sections (Krijgsman et al. 2002, Orszag-Sperber et al. 2009), located in the Psematismenos and the Pissouri basins (Fig. 1), respectively. These two sections were correlated with the Perales reference section (Sorbas basin) for the western Mediterranean (Sierro et al. 2001) by means of biomagnetostratigraphic and cyclostratigraphic constraints. Overall, the paleoceanographic evolution observed in the Cyprus basin is similar to that envisaged in the western Mediterranean, although the pre-MSC sedimentary successions differ for the scarce presence or absence of sapropels and for the occurrence of chaotic/carbonate deposits ("barre jaune") just below the lowermost gypsum bed (Kouwenhoven et al. 2006, Orszag-Sperber et al. 2009). Moreover, the identification of MSC onset in these sections has been debated. According to Krijgsman et al. (2002) and Kouwenhoven et al. (2006) it is represented by the lowermost gypsum bed in the Pissouri section. Differently, according to Orszag-Sperber et al. (2009), it coincides in the Tokhni section with the basal stromatolitic bed of the "barre jaune" and, consequently, the deposition of the lowermost gypsum bed is delayed by 60 kyrs. Both these interpretations have been questioned by Manzi et al. (2016) based on sedimentologic and stratigraphic evidences. These authors stated that on Cyprus the Primary Lower Gypsum (PLG, Roveri et al. 2009) of the 1st stage of the MSC are lacking, whereas the gypsum deposits are clastic facies floored by an angular unconformity likely corresponding to the Messinian erosional surface (MES). Thus, the gypsum unit of the Tokhni section has been ascribed to the stage 2 of the MSC (Roveri et al. 2009). Consequently, Manzi et al. (2016) suggested that MSC onset is best approximated by the last occurrence of foraminifera, identified within the interval corresponding to the "barre jaune" of Orszag-Sperber et al. (2009).

Here, we present a reinvestigation of the upper part of the Tokhni section producing an updated calcareous plankton biostratigraphy and cyclostratigraphy, validated by new magnetostratigraphic data. The micropaleontologic and isotopic data, supported by the

new age model and integrated with the stratigraphic and sedimentologic evidences as presented in Manzi et al. (2016), allowed the reconstruction of the paleoenvironmental and paleoceanographic evolutions in the Psematismenos basin during the pre-MSC and their comparison with those of the central and western Mediterranean successions.

2. Geological setting and section

The Tokhni composite section is exposed in the badlands 1 km southwest from the village of Tokhni (southern Cyprus Island), located at the southeast termination of the Troodos Massif, in the Psematismenos basin (Fig.1). The composite section combines 4 sub-sections (To-0, To-1, To-2 and To-3; Fig. 2; Manzi et al. 2016), and comprises the upper part of the Pakhna Formation (Bagnall 1960, Gass 1960, Pantazis 1967), and the evaporites of the Kalavasos Formation. Here we follow the subdivision of the Pakhna Formation into four sub-units (from the bottom, PK-A_1, PK-A_2, PK-A_3 and PK-B) as proposed by Manzi et al. (2016) (Fig. 2).

1) Sub-unit PK-A_1 – It consists of m-thick alternation of darker and lighter homogeneous blue marls. Orszag-Sperber et al. (2009) recognized the Tortonian-Messinian boundary in the upper part of this sub-unit on the basis of the first occurrence of the planktonic foraminifer *Globorotalia miotumida*.

2) Sub-unit PK-A_2 – It is characterized by a lithologic cyclic stacking pattern formed by an alternation of prominent marls and reddish shales.

3) Sub-unit PK-A_3 – It is mainly characterized by a cyclic alternation of reddish shales and whitish micritic limestones, and its base is marked by a 80 cm-thick whitish limestone bed. However, from ca. 15 m above the base of this sub-unit, marl layers and/or slightly prominent pink diatomitic layers are associated with or replace the whitish limestone within the basic cycle. Diatomites are particularly common in the upper part of this sub-unit and within the upper PK-B sub-unit (see below). The micritic limestone layers, in particular the

lowermost one, are laterally continuous and easily detectable in the field, and were used as key-beds in the reconstruction of the composite section (Fig. 2). These layers are made up of a mixture of clay and coccoliths cemented by micron-sized calcite crystals (Manzi et al. 2016). Another useful key-bed observed in the upper part of this sub-unit is a thin conglomerate layer (thickness 25-40 cm), showing an erosive base. This layer is entirely made up of limestone-derived pebbles floating in a bioclastic packstone matrix; the latter contains planktonic and benthic foraminifera, siliceous sponge spicules, echinoid spines and fragments of coralline algae. Sparse silt-size terrigenous grains are also present.

4) Sub-unit PK-B - This uppermost sub-unit has been recognized only in the southern subsections To-2 and To-3. It is characterized by the presence of 3 limestone beds (indicated as A, B and C) showing different characteristics with respect to the limestones of sub-unit PK-A_3 and intercalated by reddish shales and pink diatomites. These limestone beds belong to the “barre jaune” described in the Tokhni section by Orszag-Sperber et al. (2009), who interpreted them as precession-controlled stromatolites suggesting periodical shallowing and drying up of the basin. Differently, Manzi et al. (2016) did not recognize evidences of shallowing or drying up. According to these authors the lower part of the limestone A is a finely laminated microbialite and contains cavities possibly indicating the displacive growth of sub-millimetric gypsum crystals, successively replaced by micrite. The upper part of limestone A shows penecontemporaneous reworking of the microbialite by subaqueous gravity flows. The two uppermost limestone layers (B and C) show completely different characteristics and internal organization. They are made up of coarse-grained clastic sediments, grainstone and rudstone likely deriving from the dismantlement of a penecontemporaneous carbonate platform forming in the Tokhni area (Robertson et al. 1995).

The boundary between the Pakhna and the Kalavasos formations is sharp and discordant. In fact, as described in Manzi et al. (2016), the uppermost part of the Pakhna Formation

shows from south to north: i) the disappearance of the PKB sub-unit; ii) a progressive truncation of the PK-A_3 sub-unit (Fig. 2); iii) a steeper inclination of the base of the evaporites of Kalavasos Formation with respect to the Pakhna Formation. Accordingly, the base of the Kalavasos Formation is an angular unconformity and coincides with the Messinian erosional surface (MES); indeed, these evaporites are clastic and belong to the Resedimented Lower Gypsum (RLG, Roveri et al. 2009) unit deposited during stage 2, rather than representing the Primary Lower Gypsum (PLG of Roveri et al. 2009) of stage 1, as previously argued by Orszag-Sperber et al. (2009). In the present study we focus on the upper part of the Tokhni composite section, corresponding to sub-units PK-A_3 and PK-B.

3. Material and Methods

3.1. Magnetostratigraphy

A total of 16 samples were collected in the subsection To-1 (10 - 31.5 m interval of the composite section; Fig. 2), mainly from the limestone beds, due to the pervasive fracture of the shales and lamination of the diatomites. Samples were thermally demagnetized in an ASC electric hoven at the Alpine Laboratory of Paleomagnetism (Alp, Peveragno, Italy) and were initially heated at 100°C and then up to 340-450°C, by successive increasing steps of 30°C. At each step we measured the remanent magnetization in a 2G-Enterprises DC SQUIDS cryogenic magnetometer, and the magnetic susceptibility to check for thermal alteration of the magnetic mineralogy. The NRM data were processed with the Remasoft software (Chadima and Hrouda 2006), which computed the principal component analysis of the linear vector (Kirschvink 1980) picked from orthogonal projection demagnetization diagrams (Zijderveld 1967) to obtain the characteristic remanent magnetization (ChRM).

3.2. Foraminifera

211 The 87 samples collected from subsections To-1, To-2 and To-3 (Fig. 2) were dried and
212 then soaked in diluted H_2O_2 for a few days; successively, they were washed using a 63 µm
213 mesh, dried again and sieved to obtain the study fraction (> 125 µm). The planktonic
214 foraminifer record of the Tokhni section is biased by several problems: a) reworking of
215 Eocene to middle Miocene specimens (see also Orszag-Sperber et al. 2009) is present in
216 the PK-A_2 and lower part of PK-A_3 sub-units, up to 7 m of the composite section and it
217 gradually decreases upward; b) in the 0-28 m interval the foraminifer abundance is highly
218 variable and roughly decreases from the bottom to the top; in particular, the most
219 prominent limestones starting from 11.5 m are barren of both benthic and planktonic
220 foraminifera; c) inorganic particles (terrigenous grains, un-disaggregated sediment, etc.)
221 represent a large portion of the washed residues; d) preservation is generally poor. For
222 these reasons qualitative observations were performed on the samples collected from PK-
223 A_2 and lower part of PK-A_3 sub-units. A semi-quantitative analysis of selected taxa was
224 carried out on 48 out of 60 samples collected from PK-A_3 and PK-B sub-units (from 7 m
225 upward of the Tokhni composite section, see Fig. 2), avoiding samples barren in
226 foraminifera (limestones) and samples characterized by very diluted foraminiferal content
227 and/or very poor preservation. Among planktonic foraminifera, all the *Globigerina*,
228 *Globigerinoides* and *Globigerinita* species were respectively clustered as genera; however,
229 *Globigerina bulloides* is largely predominant within the *Globigerina* gr., and *Globigerinita*
230 *glutinata* within the *Globigerinita* gr. Sinistrally and dextrally coiled *Neogloboquadrina*
231 *acostaensis* were counted separately. Bolivinids, buliminds and elphidiids were considered
232 as generic groups among benthic foraminifera. A group of taxa showing low abundances
233 and including *Hanzawaia boueana*, *Cancris oblungus*, *Valvulineria complanata*, *Rosalina*
234 *globularis* and *Ammonia* sp. were lumped together as “inner shelf taxa”. Each selected
235 taxon was picked and counted at maximum in 9 fields (out of 45) of a standard picking tray
236 if not exceeding 30 specimens. The total abundance of planktonic and benthic foraminifera

and the abundance of the selected taxa were then normalized to one field and plotted against the stratigraphic height. We also calculated the P/B ratio as P*(P+B)/100, where P and B represent the total number of planktonic foraminifera and benthic foraminifera per field, respectively.

3.3. Calcareous nannofossils

Calcareous nannofossil assemblages from 60 out of 87 samples collected in the Tokhni composite section within PK-A_3 and PK-B sub-units (8 - 36.5 m; Figs. 2, and 5) were studied in smear slides with a microscope at 1250X under cross polarized light microscope. Slide preparation was kept simple using standard techniques in order to retain the original composition of the sediment (Bown and Young 1998). Only the uppermost samples in the studied interval were barren of calcareous nannofossils. Quantitative analyses were carried out by counting at least 500 specimens per sample and relative abundances are expressed in % of the total assemblage. Abundance percentages of significant taxa were plotted against their stratigraphic level. Frequencies of very rare and biostratigraphically significant genera (*Amaurolithus*, *Discoaster*) were estimated by counting the number of specimens in 500 fields of view, corresponding to an area of 11.250 mm^2. Abundances of these taxa are expressed in n/mm^2. *Discoaster* spp. were identified at the species level, nevertheless, due to the very low abundance of *D. surculus*, we lumped *D. surculus* and *D. variabilis* into the *Discoaster variabilis* group.

3.4. Isotopic geochemistry

3.4.1. Oxygen and Carbon stable isotopes

Stable oxygen and carbon isotope composition of 79 bulk samples were measured in the Geochemistry Laboratory of the Physical and Earth Science Department of the University of Parma. The isotopic composition of calcite samples (originating from micritic crystals,

foraminifera and calcareous nannofossils) was obtained from the reaction of the powdered carbonate with 100% H_3PO_4 “in vacuo” and under controlled temperature (25°C). The isotopic composition of CO_2 samples was measured on a Finnigan Delta S mass spectrometer against a CO_2 standard gas obtained by the reaction at 25°C of very pure Carrara marble powder with 100% phosphoric acid. The standard deviation of these measurements was systematically equal to or lower than ±0.15 ‰ (1σ). The CO_2 standard from the Carrara marble used in our laboratory is periodically calibrated against NBS-19. Its isotopic composition is -2.43 ‰ (δ^{18}O vs. VPDB) and +2.45 ‰ (δ^{13}C vs. VPDB).

3.4.2. Strontium isotopes

Samples were collected from every prominent limestone bed from 10 m upwards of the composite section and $^{87}Sr/^{86}Sr$ isotope analyses were carried out at SUERC (Scottish Universities Environmental Research Centre, East Kilbride, Scotland). Samples were leached in 1M ammonium acetate prior to acid digestion with HNO_3. Sr was separated using Eichrom Sr Spec resin. Matrix elements were eluted in 8M HNO_3 and 3M HNO_3 before elution of Sr in 0.01M HNO_3. Total procedure blank for Sr samples prepared using this method was <200 pg. In preparation for mass spectrometry, Sr samples were loaded onto single Re filaments with a Ta-activator. Sr samples were analyzed with a VG Sector 54-30 multiple collector mass spectrometer. A ^{88}Sr intensity of 1V (1 x 10 - 11 A) ± 10% was maintained. $^{87}Sr/^{86}Sr$ ratio was corrected for mass fractionation using $^{86}Sr/^{88}Sr$ = 0.1194 and an exponential law. The mass spectrometer was operated in the peak-jumping mode with data collected as 15 blocks of 10 ratios, which gives an internal uncertainty of <0.000020 (2 S.E.). For this instrument NIST SRM 987 gave 0.710249 ± 0.000008 (1 S.D., n = 17) during the course of this study. The 2 standard error internal precision on individual analyses was between 0.000014 and 0.000020 for 2σ.

289 4. Results

290 4.1. Magnetostratigraphy

291 The thermal demagnetization paths show that between the NRM and 180°C a normally
292 oriented, low temperature component is generally demagnetized. Between 180° and 340°
293 - 560°C a second component can be isolated, displaying both normal and reversed
294 polarities and thus interpreted as the characteristic component (ChRM). However, at 340°
295 C the specimens collected between 10 and 19 m still retain 10-20% of the initial NRM, and
296 a further increase of temperature usually results in randomly oriented direction and/or a
297 remanence increase. This fact indicates that a potential third component with higher
298 coercitivity also could be present, but not detected in our samples, due to the formation of
299 authigenic magnetic minerals with increasing temperature above 340°C. In the lower half
300 of the sampled subsection, To13b is the only sample showing a certain reversed ChRM
301 orientation (Fig. 3a, c). Samples To11 and To13a display reversed inclination, but the
302 declination is respectively east and west oriented (Fig. 3 b). Samples To12 and To10 were
303 discarded because the signal was too weak. In the upper part of the sampled subsection,
304 the demagnetization paths of samples To01, To05 - To08 show the presence of a more
305 stable normal ChRM isolated in a larger temperature range, between 180° and 460° -
306 560°C (Fig. 3a). Summarizing, a reversed magnetozone is pinpointed between 11 and 12
307 m; however, its top is not well defined as sample To11, which tentatively represents the
308 uppermost reversed polarity level, is included in an interval of poorly defined polarities,
309 between 12 and 21 m. A normal magnetozone is identified from 21 and 31.5 m.

310

311 4.2. Planktonic foraminifera

312 In sub-unit PK-A_2 and in the lower part of sub-unit PK-A_3, up to 7 m from the base of the
313 composite section (Fig. 2), preservation varies from poor to moderate and deformation
314 and/or incrustation commonly prevents the classification of foraminifera at the species

level. Inorganic grains (mainly terrigenous particles and un-disaggregated marly sediment) are often abundant and regardless of the lithology can be prevalent on the fossil remains. Foraminifera are usually more abundant in the marls than in the reddish shales, and planktonic foraminifera are generally more common than the benthic. A common feature is the presence of reworked Eocene to middle Miocene taxa, probably derived from the erosion of the uplifted carbonate formations (Lefkara and Pakhna formations) widespread on the Island of Cyprus (Robertson et al. 1995). In this interval, *Globigerinoides* spp. and *Orbulina universa* are generally the most common taxa, among the planktonic foraminifera, followed by neogloboquadrinids (mainly sinistrally coiled), *Globigerinita glutinata* and *Globigerina bulloides*.

Semi-quantitative analyses, performed from 7 m of the composite section upward (Fig. 4), indicate that the abundance pattern of foraminifera is characterized by the occurrence of successive peaks, mainly observed in the reddish shales, and that from 11.5 m upward almost all the prominent limestones are devoid of foraminifera (except at 14.6 m, where *O. universa* occurs). Abundance of planktonic foraminifera first drops above 22 m, where peaks are less prominent and then, just above the conglomerate bed at 31 m, where foraminifera become scattered (Fig. 4). As shown by the P/B ratio, planktonic are generally much more abundant than benthic foraminifera in the interval from 7 to 15.5 m; upward, the ratio fluctuates with no evident relationship with lithology.

From 7 m upward, planktonic foraminifer assemblages are more oligotypic with respect to the lower part of sub-unit PK-A_3. The genus *Turborotalita* is rather common, even though discontinuously distributed (Fig. 4). *T. quinqueloba* prevalently occurs in the shales, but it is also present in the thin limestone bed at 10 m and in the marl at 23 m. It also shows few prominent abundance peaks, reaching up to 100 specimens/field in a monospecific assemblage at 10 m and at 26.5 m. *T. multiloba* first occurs (FO) at 10.2 m and is characterized by a very scattered distribution and generally low abundance in the shales,

while it is quite common (up to 20-30 specimens/field) only in the limestone layer at 10.2 m and in a marly level at 23.25 m (abundance influx, Ai). *T. multiloba* last occurs (LO) at 31 m, just above the conglomerate (Fig. 4).

The *Globigerinita* gr. is relatively common between 8 and 21 m (Fig. 4), attaining abundance maxima at 16 and 21 m; upward, it is very scattered and it disappears above the conglomerate layer at 31m.

The distribution range of the *Globigerina* gr. is similar to that of the *Globigerinita* gr. (Fig. 4); however, it is only abundant in the shale at 9 m and, differently from the latter, it disappears at about 34.5 m, just above the lowermost limestone bed of sub-unit PK-B, i.e. at the stratigraphic level of the last recovery of planktonic foraminifera.

Neogloboquadrina acostaensis is usually rare (< 5 specimens/field) except at 25.5 m (35 specimens/field). The Last regular influx of sinistrally coiled individuals (Lri of Sierro et al. 2001) is recognized at 12.6 m, while at 13.5 m dextrally and sinistrally coiled specimens occur equally (Fig. 4). Dextrally coiled *N. acostaensis* prevails from 15.25 m (first abundant occurrence, FAO, of Sierro et al. 2001) and is quite regularly present up to 19.5 m. This taxon is more scattered upwards, vanishing at about 33.5 m, just below the base of sub-unit PK-B (Fig. 4).

Globigerinoides spp. is subordinated, showing few minor peaks (<20 specimens/field) between 11 and 20 m and disappear above 25.5 m (Fig. 4). *O. universa* is irregularly distributed along the composite section and is abundant only between 13 and 14.5 m (where it is also common in a prominent limestone layer). *Globorotalia scitula* is present with rare individuals at 29.7 m (Gs influx in Fig. 4). It is worth observing that the topmost planktonic foraminifer assemblage is represented by *O. universa*, *N. acostaensis* and *Globigerina* gr. and the last recovery of planktonic foraminifera (LRp) occurs at 34.5 m.

4.3 Benthic foraminifera

In sub-unit PK-A_2 and the lower part of sub-unit PK-A_3 up to 7 m of the composite section, the presence of benthic foraminifera is generally subordinate to planktonic ones and mainly represented by *Elphidium* spp, *Neoconorbina orbicularis*, *Rosalina globularis*, *Valvulineria complanata*, *Melonis* sp., *Gyroidinoides* sp., *Cibicides* spp., *Cibicidoides* spp., *Bolivina* gr. (mainly *B. spathulata* and *B. dilatata*), *Bulimina* gr. (mainly *B. aculeata*, *B. echinata* and *B. elongata*), *Hanzawaia boueana*, *Cancris oblungus* and *Uvigerina bononiensis*.

From 9 m of the Tokhni composite section upward, the benthic assemblages become prevalently dominated by the *Bolivina* gr. (mainly *B. dilatata* and *B. spathulata*), which is particularly abundant in the 15.5 - 28 m interval, where it peaks in the shales in correspondence to the P/B minima (Fig. 4). Benthic foraminifera are absent in the limestone beds from 11 m upward, and scattered or absent in some shale levels. A marked abundance decrease is observed from 28.5 m up to 35.2 m, where the last recovery of benthic foraminifera (LRb), represented by the *Bolivina* gr., is recorded. In the benthic abundance peaks, the *Bolivina* gr. is commonly associated with subordinated buliminids, *Elphidium* spp. and with the inner shelf taxa group (*H. boueana*, *C. oblungus*, *V. complanata*, *R. globularis* and, rarely, *Ammonia* sp.). These generally subordinated taxa represent major components of the assemblages just in two samples, at 18 and 25 m (Fig. 4).

4.4. Calcareous nannofossils

Calcareous nannofossil assemblages in the upper part of sub-unit PK-A_3 and sub-unit PK-B, from 7 m up to the top of the composite section, show moderate to poor preservation. In general, preservation within the micritic limestone layers is poorer than in the shale intervals. Calcareous nannofossils are common to abundant along the section but decrease in abundance at 28.3 m and at 34 m (Fig. 5); however they are still present up to

393 the uppermost sample at 36.5 m. Reworking of calcareous nannofossils from sediments as
394 old as Early Cretaceous occurs sporadically and mainly in the reddish shales of each cycle.
395 However, abundance of reworked specimens is very low and does not hinder the
396 quantitative analysis of the assemblages. Diatoms were also detected in the smear slides
397 prepared for calcareous nannofossil analyses and occur, with discontinuous abundances,
398 from 12.2 m upward; remarkably, limestones were devoid of diatoms (R. Jordan, pers.
399 comm., 2014).
400 Major component of the fossil assemblages along the entire section are Reticulofenestrids
401 (*Reticulofenestra minuta*, *R. haqii*, *R. pseudoumbilicus*, which represent up to 80% of the
402 total assemblage), together with *Sphenolithus abies* (up to 80%), *Calcidiscus leptoporus*
403 (up to 70%) and *U. jafari* (up to 45%) (Fig. 5). *R. minuta* is present in both the limestones
404 and in the middle/upper part of the shales; however, in the latter it retains the abundance
405 maxima. Differently, *S. abies* is virtually absent in the limestones and generally shows
406 greater abundance in the lower part of the shales. The greater abundance of *Cd.*
407 *leptoporus* occurs in the limestone layers up to 29.25 m; above this level its abundance
408 drops to less than 5% and it is replaced by *Reticulofenestra antarctica* within the
409 limestones up to 32.5 m. *U. jafari* is prevalently present with abundance peaks in the
410 limestones up to 31 m, where it disappears.
411 *U. rotula* is a minor component (with peak close to 18%) of the assemblage up to 34 m,
412 but it reaches 90% in the abundance peak (Ap) between limestones A and B of PK-B sub-
413 unit (35 m) (Fig. 5). *Helicosphaera carteri* shows low abundances up to 26 m, reaching
414 15% of the total assemblage at 34.5 m. *Discoaster* spp. occurs from the bottom of the
415 section and the *Discoaster variabilis* gr. (< 5%) is quite regularly present in three intervals:
416 10 - 12 m, 18 - 21 m and 25.5 - 29.5 m. It is prevalent in the shales, but it also occurs in
417 the lower part of the limestones at 11.5 m and at 26 m. *Braarudosphaera bigelowii* shows

418 an abundance peak (130 n/mm^2) at 25.8 m (Fig. 5), being otherwise absent below and
419 above this layer.
420 The biostratigraphically useful taxa *Amaurolithus delicatus* and *A. primus* are generally
421 very rare and shows very scattered occurrences.
422
423 4.4. Isotopic geochemistry ($\delta^{18}O$, $\delta^{13}C$ and $^{87}Sr/^{86}Sr$)
424 Oxygen isotope values (Fig. 6) range from -4.57‰ to 2.49‰ (PDB), showing a cyclic
425 stacking pattern with heavier values in the limestones and lighter values in the reddish
426 shales and pink diatomites. The heaviest values are observed in the limestones below 9
427 m; a shift towards more depleted values is recorded between 9 and 18.5 m, both in the
428 limestones and in the shales. From 18.5 up to 34 m (base of sub-unit PK-B) positive and
429 negative values of $\delta^{18}O$ quite regularly match with the limestones and shales, respectively,
430 however, relative maxima close to zero are documented between 26.5 and 28.5 m. At 34
431 m a sudden drop towards the most negative values of the succession is observed; minima
432 occur in the grey and pink shales, while the uppermost three carbonates show values
433 close to zero. Carbon isotope values are prevalently negative, ranging from -3.19‰ to -
434 0.5‰ (PDB), without any evident relationship with lithology (Fig. 6). Just one positive peak
435 at 0.51‰ was measured in the lowermost limestone of the sub-unit PK-B. However, a
436 covariance is observed in the long-term trends between the oxygen and the carbon
437 curves: an increase from the bottom to 4.5 m is followed by an overall decrease down to a
438 minimum at 16 m. Upward an increasing trend is recorded up to 22 m, where a relative
439 maximum of -0.74‰ occurs. Further up, values range between -2 to -1‰ and are
440 punctuated by a positive peak corresponding to the laminated portion of the lowermost
441 carbonate of sub-unit PK-B. As the lowermost carbonate of sub-unit PK-B is laminated, we
442 measured the isotope ratios for two white and brown consecutive laminas. Remarkably,
443 the isotopic signatures of these two laminae are different, as we obtained $\partial^{18}O$ and $\partial^{13}C$

444 values of -1.31‰ and -0.58‰ for the white and of 0.17 ‰ and 0.51 ‰ for the brown
445 lamina, respectively.
446 The $^{87}Sr/^{86}Sr$ isotopic ratio is generally slightly greater than that of the oceanic mean
447 values (Mc Arthur et al. 2001) in sub-unit PK-A_3 (Fig. 6), except for samples at 20.25, 24.5
448 and 32.5 m. Conversely, in sub-unit PK-B the isotopic ratio gradually decreases below the
449 oceanic values, showing two minima in the clastic limestones B and C.
450
451 5. Discussion
452 5.1. Biomagnetostratigraphy
453 In terms of planktonic foraminiferal biostratigraphy, the FO of *T. multiloba* (dated at 6.415
454 Ma in the Perales section by Sierro et al. 2001) at 10.2 m, the Lri of *N. acostaensis* with
455 predominant sinistral coiling (6.378 Ma; Sierro et al. 2001) at 12.6 m, the FAO of dextrally
456 coiled *N. acostaensis* (6.339 Ma; Sierro et al. 2001) at 15.25 m allow us to assign the
457 middle and upper part of PK-A_3 sub-unit to the Messinian biozones MMi13b and MMi13c
458 of Iaccarino et al. (2007). The MMi13b/MMi13c subzonal boundary is defined by the coiling
459 change of *N. acostaensis* between 12.6 and 15.25 m. The succession of these events also
460 indicates that discontinuous reversed polarity samples recorded between 11 and 12 m and
461 at 17 m are referable to the C3An.1r sub-chron (Sierro et al. 2001). In the upper part of the
462 composite section, the influx of *G. scitula* (29.7 m) and the LO of *T. multiloba* (31 m) occur
463 within a normal polarity magnetozone. The same succession of events is observed in the
464 Perales section, where they occur within sub-chron C3An.1n and are respectively dated at
465 6.102 and 6.04 Ma (Sierro et al. 2001). Thus, the influx of *G. scitula* at 29.7 m can be
466 correlated to its 2nd influx recognized in the Perales section (Sierro et al. 2001) and the
467 normal magnetozone between 22 and 31.5 m is correlated to sub-chron C3An.1n. The LR
468 of planktonic and benthic foraminifera between limestones A and B in the sub-unit PK-B
469 marks the base of the Non-Distinctive Zone (NDZ) of Iaccarino et al. (2007) and are

470 considered as a good approximation of the MSC onset. In fact, the LR of planktonic (LRp)
471 and benthic (LRb) foraminifera (> 125 μm) have been recognized in the penultimate cycle
472 (Perales, Falconara, Legnagnone) and in the last cycle of the pre-MSC unit (Perales,
473 Legnagnone), respectively (Blanc-Valleron et al. 2002, Gennari et al. 2013, Manzi et al.
474 2011, 2013, Sierro et al. 2003). In the Pollenzo section the LRp and the LRb (>125μm)
475 have been recognized in the 1st and 2nd PLG cycles, respectively (Violanti et al. 2013), but
476 a strong decrease in the foraminiferal abundance marks the onset of the MSC.
477 Regarding calcareous nannofossils, the occurrence of *A. delicatus* and *A. primus* from the
478 bottom of the composite section, albeit scattered, indicates the presence of the MNN11b/c
479 biozones (Raffi et al. 2003). In addition, recently, calcareous nannofossil bioevents have
480 been identified associated with the onset of the MSC in the Northern Apennine (Manzi et
481 al. 2007, Dela Pierre et al. 2011, Violanti et al. 2013). For instance, , a sharp abundance
482 peak of *S. abies*, associated with abundant *H. carteri* and shortly followed by an
483 abundance peak of *U. rotula* close to 60% of the assemblage, is reported in the Pollenzo
484 section (NW Italy) in the sediments deposited during the first Primary Lower Gypsum
485 (PLG) cycle (Lozar et al. 2010 and this volume, Violanti et al. 2013). Remarkably, both at
486 Pollenzo and in the Fanantello borehole (Northern Apennine, Italy; Manzi et al. 2007), *S.*
487 *abies* shows low abundances all over the section, with a noticeable 60% abundance peak
488 at the base of the first PLG equivalent cycle. In the Tokhni section, on the contrary, this *S.*
489 *abies* peak is not unambiguously detectable since this taxon is abundant and regularly
490 occurs in all the shales. However, the occurrence of the sharp increase in abundance of
491 both *H. carteri* and *U. rotula* at 34.5 and 35 m respectively, close to the LR of planktonic
492 and benthic foraminifera, shows their reliability to approximate the onset of the MSC.
493
494 5.2. Cyclostratigraphy

The Tokhni section presents a well-defined cyclic lithologic stacking pattern. The cycles of sub-unit PK-A_3 are generally made up of reddish shales and prominent whitish limestones. However, while the shaley hemicycle is a constant feature of the sedimentary cycles along all the composite section, limestones can be associated with or replaced by marls and/or pink diatomites. In the sub-unit PK-B the recognition of sedimentary cycles is complicated by the clastic nature of the limestones A (upper part), B and C. This suggests that they should not be considered equivalent to the limestones of the sub-unit PK-A_3 (see Manzi et al. 2016). On the whole, in the Tokhni composite section from 7 m up to the base of the gypsum deposits, we identified 25 cycles (Fig. 7); the thickness of these cycles is rather variable and ranges from 0.5 m (cycle 21) up to 2 m (e.g., cycles 2 and 8). The occurrence of 16 cycles in a time interval of 340 kyr (between the FO of *T. multiloba* and the 2nd influx of *G. scitula*) implies an average duration of 21 kyr for each cycle, suggesting a relationship with precession, as previously observed by Orszag-Sperber et al. (2009) Because of the absence of sapropels and the scarcity of diatomites, the sedimentary cycles at Tokhni are more similar to those of the Pissouri section described as an alternation of carbonates (insolation minima) and marls (insolation maxima) (Krijgsman et al. 2002) than to other pre-MSC cycles. In particular, they differ from a) the tripartite cycles of the Falconara and Gavdos sections (Blanc-Valleron et al. 2002, Perez-Folgado et al. 2003), where sapropels and marls, intercalated by diatomites are tied to insolation maxima and minima, respectively; b) the quadripartite cycles of Sorbas basin, where the sapropel is correlated to insolation maxima and followed by lower marl, diatomite and upper marl (insolation minima) (Sierro et al. 2001, 2003).

The cyclicity at Tokhni is also emphasized by fluctuations of the oxygen isotope values and of the abundance of several calcareous nannofossil taxa. In fact, heavier $\delta^{18}O$ values are associated with limestones and marls, indicating more arid and/or colder conditions, while lighter values are recorded in shales and diatomites, pointing to more humid and/or

warmer conditions (Fig. 6). These oscillations were also observed in the bulk sample stable isotope record of Falconara section (Blanc-Valleron et al. 2002), where the heavier and lighter values respectively correspond to marls/diatomites (insolation minima) and to sapropels (insolation maxima) (see also Hilgen and Krijgsman 1999). Regarding calcareous nannofossils, shales are characterized by the occurrence of *S. abies*, and *R. minuta*, (dominant in the lower/middle and upper part of the layer, respectively), both sporadically associated with less abundant *D. variabilis* gr (<5%). This assemblage is strikingly similar to that observed in the sapropels of the Sorbas basin (Flores et al. 2005). Thus, the calcareous nannofossil assemblages and the lighter $\delta^{18}O$ values suggest the correlation between the reddish shales of the Tokhni composite section and insolation maxima (Fig. 7).

Cd. leptoporus and *U. jafari* are the main components of the calcareous nannofossil assemblage in the limestones and marls up to 29.5 m and their co-occurrence was also observed in the upper marls of the Sorbas basin, correlated with insolation minima (Sierro et al. 2003, Flores et al. 2005). Thus, the occurrence of these two taxa and the heavier $\delta^{18}O$ suggest the correlation between the limestones of the Tokhni composite section and insolation minima.

5.3. Age model

To reconstruct the age model for the Tokhni composite section the biomagnetostratigraphic framework has been used for the correlation to the astronomically calibrated Messinian reference sections of Pollenzo, Perales and Falconara (Fig. 7). The calcareous plankton events have been used as tie points and the sedimentary cycles have been correlated to the 65°N summer insolation curve (Laskar et al. 2004), on the basis of the phase relation above exposed (Fig. 7). The resulting age model fits well with the 100 kyr eccentricity cycle, reflected in the intervals of low and high amplitude variations of the

summer insolation curve, corresponding to eccentricity minima and eccentricity maxima, respectively. In particular, the thick limestone of cycle 3 corresponds to the high amplitude insolation cycle at ca. 6.4 Ma; the thick cycles 8, 9 and 10 well correlate with the cluster of high amplitude insolation cycles centred at 6.3 Ma; the prominent limestones of cycle 13 and 14 well fit with the high amplitude insolation cycle at 6.2 Ma. Indeed, eccentricity minima (6.36, 6.14, 5.97 Ma) can be identified in the sedimentary record for the absence of prominent limestones, replaced by thin marls or pink diatomites (cycles 5, 15-16 and 23; Fig. 7). Moreover, the oxygen isotope curve also displays overall lighter values and smoother oscillations in both the 6.36 and 6.14 Ma eccentricity minima. The sedimentary response to the 100 kyr eccentricity cycle is a good constraint for the proposed age model; however, an additional tie point could be represented by the influx of *T. multiloba* in the 15 - 29.5 m interval, where the C3An.1r/C3An.1n reversal is poorly constrained and standard bioevents are lacking (Fig. 7). This bioevent occurs at the base of the sub-chron C3An.1n, five precessional cycles above the FAO of dextrally coiled *N. acostaensis* and six cycles below the 2nd influx of *G. scitula*. In the same stratigraphic position, in the Perales and Falconara successions (Sierro et al. 2001, Blanc-Valleron et al. 2002) *T. multiloba* show a very prominent influx (up to 100% of the assemblage), which marks a paracme end dated at 6.21 Ma, based on its occurrence in the upper part of cycle UA23 of Sierro et al. (2001).

In the upper part of the composite section, the relative position of the LO of *T. multiloba* with respect to the 2nd influx of *G. scitula* (within sub-chron C3An.1n) indicates that an erosion of ca. 2 sedimentary cycles is associated with the base of the conglomerate at 30.5 m (Fig. 7). In fact, at Tokhni, these events are recorded in two consecutive sedimentary cycles, i.e. below and above the conglomerate, while in the Perales section they are separated by three insolation minima (Sierro et al. 2001).

The proposed age model indicates that the onset of the MSC at 5.971 Ma (Manzi et al. 2013) occurs between the two lowermost limestones of the sub-unit PK-B (Manzi et al.

2016), ca. 4 precessional cycles above the LO of *T. multiloba* and well approximated by the LR of benthic and planktonic foraminifera and by the abundance peaks of *U. rotula* and *H. carteri*. In this interval the sedimentary cyclicity is poorly defined by the thin alternation of shales and diatomites due to the concomitant eccentricity minima.

Moreover, the identification of the MSC onset at ca. one precessional cycle below the MES (5.60 Ma, Krijgsman et al. 1999a) implies a hiatus of ca. 350 kyr, due to the erosion of most of the sediments associated with Stage 1 of the MSC.

5.4. Paleoenvironmental reconstruction

5.4.1. Interval 1: pre 6.4 Ma

In the lower part of the section, prior to 6.4 Ma, benthic foraminifer assemblages are similar to those recorded in the 7.16 - 6.4 Ma interval of the Pissouri section (Kouwenhoven et al. 2006). They include genera typically representative of an inner shelf to upper bathyal habitats (Murray 2006). The presence of inner shelf genera, such as *Elphidium*, *Neoconorbina*, *Rosalina* and *Ammonia*, as well as of older foraminifera, is interpreted as due to downslope transport, a process commonly observed in the pre-MSC successions of Crete and Cyprus (Van der Zwaan 1982, Kouwenhoven et al. 2006).. Thus, the diversified benthic foraminifer assemblages and the common occurrence of ostracods indicate an upper bathyal paleoenvironment and the prevalence of an oxygenated sea floor (Boomer and Eisenhauer 2002). Still, the relative high abundances of the *Bolivina* and *Bulimina* groups at some levels point to episodes of enhanced nutrient availability and lower oxygen levels (Jorissen 1987, Kahio 1994). The prevalence of *Globigerinoides* spp. and *O. universa* in the planktonic assemblages of the basal portion of the Tokhni composite section suggests overall warm and oligotrophic conditions in the upper water column (Fig. 8). The occurrence of *T. quinqueloba*, *T. multiloba* and of *G. bulloides* from

598 cycle 2 (6.44 Ma) upwards documents the establishment of more eutrophic conditions
599 (Sierro et al. 2003).
600
601 5.4.2. Interval 2: 6.4 - 6.1 Ma
602 From 6.4 Ma, the shales are characterized by the dominance of the opportunistic *Bolivina*
603 (mainly *B. spathulata* and *B. dilatata*) and, subordinately, *Bulimina* groups (mainly *B.*
604 *echinata* and *B. aculeata*), which co-occur with inner shelf benthic foraminifera and with
605 abundant sponge spicules (Fig. 8), both considered the result of downslope transport. The
606 autochthonous fauna indicates bottom waters characterized by high organic matter supply,
607 low oxygen levels and, according to Kouwenhoven et al. (2006), also by increased salinity.
608 The disappearance of ostracods also points to substantial oxygen decrease at the sea
609 bottom, whereas the abundance of sponge spicules either reveals increased availability or
610 optimal preservation of silica. These changes occurred synchronously in the adjacent
611 Pissouri basin and we infer that they are related to the establishment of stressed condition
612 at the sea floor (Kouwenhoven et al., 2006), rather than a shallowing upward trend (see
613 also Orszag-Sperber et al. 2009).
614 This interval in the Mediterranean is usually characterized by increased oscillations of the
615 P/B ratio (0 - 100%) indicating the establishment of precession-paced anoxic bottom water
616 conditions (insolation maxima) and stressed surface waters (hypertrophic/high salinity)
617 during insolation minima (Blanc-Valleron et al. 2002, Sierro et al. 2003; Kouwenhoven et al.
618 2006). At Tokhni, as well, we observe an increased response to the insolation index, which
619 involves marked micropaleontologic differences between the shales (insolation maxima)
620 and the limestones (insolation minima). However, a clear relation between assemblage
621 composition and lithology is only shown by calcareous nannofossils, as foraminifera are
622 generally only present in the shales and do not show a regular distribution pattern.

623 The shaley hemicycles record the association of the aforementioned opportunistic benthic
624 foraminifera with *S. abies*, *D. variabilis* gr., *R. minuta* and with lighter $\partial^{18}O$ values. In the
625 Atlantic Ocean Pliocene record and in the Messinian sapropels of the Sorbas basin,
626 *Discoaster* spp. and *S. abies* positively respond to low nutrient availability in the lower
627 photic zone (LPZ) and to warm sea surface temperatures (Gibbs et al. 2004a, Flores et al.
628 2005). *R. minuta* is an opportunistic taxon tolerating wide ecological changes and
629 blooming in nutrient-rich surface waters (Aubry 1992, Flores et al. 1995); in particular, the
630 increase of small sized *Reticulofenestra* has been correlated with increased riverine input
631 in the Caribbean Pliocene record (Kameo 2002) and, associated with a decrease of
632 *Discoaster*, has been related to meso- to eutrophic condition in the Late Miocene Pacific
633 record (Imai et al. 2015). In the lower/middle part of the Tokhni shales the occurrence of *R.*
634 *minuta* associated with dominant *S. abies* and rare specimens of the *D. variabilis* gr.
635 suggests that at times of insolation maxima *R. minuta* could thrive in the upper photic zone,
636 where high nutrient levels were mainly provided through increased continental runoff,
637 which also favoured the stratification of the water column. More oligotrophic condition
638 prevailed in the LPZ favouring the proliferation of *S. abies* and, to a minor extent, of *D.*
639 *variabilis* gr. In the upper part of the shales, *R. minuta* becomes dominant (40-60%),
640 generally following a drop in abundance of *S. abies*. Similar to the Sorbas basin (Flores et
641 al. 2005), this could indicate increasing nutrient availability in the surface layer immediately
642 after the insolation maxima, when the transition to a more arid condition, typically
643 established during insolation minima, favoured the onset of deep/intermediate water
644 ventilation.
645 Therefore, by analogy with the formation of the Late Miocene and Plio-Pleistocene
646 sapropels (Nijenhuis et al. 1996), we argue that continental runoff increased during
647 insolation maxima, triggering the stratification of the water column and raising nutrient and
648 silica levels. The oxygen consumption at the sea floor was favoured by the elevated

649 organic matter levels supplied directly from the continent and from the primary productivity
650 in the photic zone (Fig. 8). The combination of these processes favoured the formation of
651 dysoxic or anoxic bottom waters, as indicated by abundance peaks of the *Bolivina* and
652 *Bulimina* groups and levels with scarce or absent benthic foraminifera. Differently, benthic
653 foraminifera are completely absent in sapropels deposited after 6.4 Ma in the Western
654 Mediterranean Perales section, indicating the establishment of more permanent sea floor
655 anoxia in response to a stronger density stratification of the water column at times of
656 insolation maxima (Sierro et al. 2003).
657 In the marls and limestones of this interval *Cd. leptoporus* occurs with *U. jafari*, while,
658 remarkably, foraminifera are generally absent. The possibility that dissolution had altered
659 the micropaleontologic record of the limestones is regarded as unlikely, since the co-
660 occurrence of the very resistant *Cd. leptoporus* (McIntyre and McIntyre 1971, Dittert et al.
661 1999, Ziveri et al. 2007) with the very delicate *U. jafari* (Gibbs et al. 2004b), recorded in
662 abundances higher than 30%, is taken as indication of minor diagenetic effects on the
663 assemblage.
664 Extant *Cd. leptoporus* has broad ecological preferences and opportunistic behaviour
665 (Renaud et al. 2002, Boeckel et al. 2006, Baumann et al. 2016). In fact, it is related to
666 warm/temperate waters with higher nutrient input to the upper photic zone and a shallower
667 nutricline, possibly driven by effective mixing due to upwelling (Ziveri et al. 2004, Ausin et
668 al. 2015). *Cd. leptoporus* is abundant and associated with small placoliths (i.e. small
669 Reticulofenestrids) in the basal homogeneous marls of each cycle of the pre-MSC Serra
670 Pirciata and Torrente Vaccarizzo sections (Caltanissetta Basin, Sicily; Bellanca et al.
671 2002), where it co-occurs with *T. quinqueloba* and *N. acostaensis*, indicating cooler and
672 eutrophic waters. At Sorbas, *U. jafari* can be abundant in the upper marls (insolation
673 minima) and is inferred to tolerate high salinity (Flores et al. 2005).

674 The presence of these taxa together with the heavier $\partial^{18}O$ values suggest that during
675 insolation minima the higher evaporation rate increased the sea surface salinity, favouring
676 the mixing of the water mass, the formation of deep/intermediate waters and triggering
677 eutrophic conditions in the upper part of the water column. This mechanism is similar to
678 that allowing the formation of the Levantine Intermediate (and Deep) Water, which, at
679 present, originates in winter in the Cyprus-Rhodes Area and resides between 150 and 600
680 m in the Eastern Mediterranean (Rohling et al. 2015). Notably, the absence of *U. jafari* and
681 the lighter $\partial^{18}O$ in the intervals correlated to eccentricity minima (cycles 6-7, 11 and 15-17)
682 could indicate that the lowered seasonality decreased the formation rate of highly saline
683 superficial waters. Note, however, that the relatively lighter $\partial^{18}O$ maxima measured in the
684 limestones of these intervals may be also related to the abundance of *Cd. leptoporus* in
685 these layers, as this species is known to calcify at negative disequilibrium with the original
686 sea water (Dudley and Nelson, 1989, Ziveri et al. 2003, Hermoso et al. 2014).
687 The absence of benthic and planktonic foraminifera in almost all limestones of this interval
688 represents a peculiarity of the Tokhni section with respect to the Mediterranean pre-MSC
689 successions. In the adjacent Pissouri basin a-planktonic layers occur; however, their origin
690 and relation with the insolation index remains unclear (Kouwenhoven et al. 2006). In the
691 coeval portion of the Sorbas basin planktonic foraminifera solely can be absent or strongly
692 reduced during insolation minima, while benthic foraminifera show abundance maxima
693 (Sierro et al. 2003). The authors speculated that the absence of planktonic foraminifera
694 could be explained by the highly eutrophic, relatively toxic waters supplied to the photic
695 zone during phase of intense mixing. This explanation could hold true for the Tokhni
696 limestones; however the higher abundances of *U. jafari* and the heavier $\partial^{18}O$ values also
697 suggest that highly saline waters formed in the superficial layer could have prevented the
698 proliferation of planktonic foraminifera. The advection of the newly formed highly saline
699 waters to the sea floor, could have created unfit conditions for benthic foraminifera, too.

700

701 5.4.3. Interval 3: 6.1 - MSC onset

702 After 6.1 Ma planktonic and benthic foraminifera show a drop in abundance also in the
703 shales, indicating increasingly stressed environmental conditions. However, the benthic
704 assemblage composition remains the same and, together with the presence of shelf to
705 bathyal cuspidariids bivalves in the sub-unit PK-B (Manzi et al. 2016), indicates that no
706 remarkable paleodepth variation occurred in the proximity of the MSC onset, similarly to
707 the Pissouri basin (Kouwenhoven et al. 2006). Conversely, calcareous nannofossil
708 assemblages record important variations (Fig. 8). The *D. variabilis* group, *P. japonica*, *U.*
709 *jafari*, and *Cd. leptoporus* vanish, while *R. antarctica*, *H. carteri* and *U. rotula* show a
710 remarkable abundance increase.

711 In this interval, the shales are still characterized by *S. abies* and *R. minuta* but not *D.*
712 *variabilis* gr. This assemblage could suggest a shallower nutricline (being *Discoaster* spp.
713 adapted to the lower photic zone, like the extant *Florisphaera profunda*; Flores et al. 2005,
714 Stoll et al. 2007) and a moderate nutrient availability. Strong changes in sea surface
715 salinity are also envisaged, since *S. abies* has been reported to be common to abundant
716 between the gypsum beds of Stage 3 of Roveri et al. (2009), suggesting that it could be an
717 euryhaline taxon (Polemi basin, Cyprus; Wade and Bown 2006). The continuous cyclic
718 abundance of *S. abies* after 6.1 Ma confirms that the latter taxon shares only some
719 ecological preferences with *D. variabilis* gr.

720 *Cd. leptoporus* and *U. jafari* are replaced in the limestone beds by *R. antarctica*, a
721 *Reticulofenestra* species characterized by closed central area. Such Reticulofenestrids are
722 also documented by Krhovsky et al. (1992) from diatom-rich Oligocene sediments from the
723 Czech Republic (Uhercice Fm. and Dynow Marlstone), where they co-occur with fresh to
724 brackish water diatom species *Melosira* (*Aulacosira*) indicating that this taxon and its
725 relatives could flourish in eutrophic environments with brackish to normal marine salinity.

In the topmost samples (across and above the MSC onset) planktonic foraminifera are nearly absent and calcareous nannofossils assemblages become increasingly dominated by *S. abies*, *R. minuta*, *U. rotula*, and to a lesser extent *H. carteri*. *H. carteri* is a meso- to eutrophic taxon (Ziveri et al. 2004), reported from eutrophic, hyposaline waters (Giraudeau 1992, Flores et al. 1997) and estuarine environments (Cachão et al. 2002). This taxon commonly occurs in the clays of the Upper Gypsum unit of Stage 3 of the Polemi basin together with *Umbilicosphaera* specimens that were interpreted as high salinity taxa (Wade and Bown 2006). In the Tokhni section high abundances of *U. rotula* occur both together and just above the *H. carteri* abundance peak, suggesting on the contrary that *Umbilicosphaera* spp. could be euryhaline and thrive in abnormal salinity waters. As for *R. minuta*, small Reticulofenestrids are also particularly abundant in the sediments deposited at the beginning of the MSC in the Piedmont Basin, testifying their tolerance to stressed (Lozar et al. 2010, Violanti et al. 2013) and nearshore environments (Perch-Nielsen 1985), characterized by eutrophic surface waters and variable salinity. The association of *U. rotula* and *R. minuta* with *H. carteri*, the distinct negative $\partial^{18}O$ values and the decline of the $^{87}Sr/^{86}Sr$ ratio (Fig. 8), which indicates a marked decreased influence of oceanic-derived waters, typical of the Stage 1 deposits (Roveri et al. 2014), suggest a preference of these taxa for lowered salinity. All this evidence indicates that the deposition of the conglomerate, coeval to the 6.1 Ma Mediterranean paleoceanographic step, marked an increasing riverine influence, both during insolation minima and maxima, reaching an acme at the MSC onset. The conglomerate is coeval to the slurry bed deposited in the Pissouri basin (Krijgsman et al. 2002, Manzi et al. 2016) and to a similar layer observed in the Fanantello borehole, which marks an increase of the terrigenous input into the Northern Apennine foredeep. Slope instability is also recorded in the Piedmont basin just below the LO of *T. multiloba* (Lozar et al. 2010, Violanti et al. 2013). These evidences suggest that a tectonic

751 impulse, likely affecting the Eastern and Northern Mediterranean, could have contributed
752 to trigger the paleoceanographic changes observed at ca. 6.1 Ma.
753
754 5.5. Paleohydrologic implication for the *Braarudosphaera bigelowii* peak
755 *Braarudosphaera bigelowii* has a very scattered but continuous occurrence along the
756 geological record since the Early Cretaceous and shows sporadic blooms as that recorded
757 at 26 m (up to 130 n/mm^2) in the Tokhni composite section (Fig. 5). It has often been
758 related to neritic environments (Bown et al. 2005, Bartol et al. 2008), to nutrient enrichment
759 and/or low salinity waters, and is generally absent in oceanic settings (Peleo-Alampay et al.
760 1999, Kelly et al. 2003, Bartol et al. 2008). The affinity of *B. bigelowii* for hypohaline waters
761 is well illustrated by its presence in the Black Sea, where surface waters have an average
762 salinity of 17‰ to 18‰, and by its absence in the high-salinity waters of the Red Sea
763 (Bukry 1974). This episodic occurrence suggests a sporadic and transient supply of
764 fresher waters, either from enhanced runoff or from the connection with a brackish/fresh
765 water body. The stratigraphic position of this abundance peak, three cycles below the 2nd
766 influx of *G. scitula,* dated at 6.102 Ma (correlated to cycle UA27 in the Abad composite,
767 Sierro et al. 2001), suggests that these low salinity waters could have been sourced from
768 the paleo-Black sea, during the transient connection of the two basin approximating the
769 Meotian/Pontian boundary (Grothe et al. 2014, Vasiliev et al. 2015).
770
771 6. Conclusions
772 The Tokhni composite section (Psematismenos basin, southern Cyprus Island) is
773 characterized by the precession-paced alternation of red shales (precession
774 minima/insolation maxima) and limestones (precession maxima/insolation minima). The
775 phase relation between sedimentary cycles and precession cycles is based on cyclic
776 variations of calcareous nannofossil taxa and ∂^{18}O values. The planktonic foraminifer and

777 magnetostratigraphic events set the tuning of the sedimentary cycles to the 65°N summer
778 insolation curve and to the Mediterranean pre-evaporitic reference sections (Sierro et al.
779 2001, Blanc-Valleron et al. 2002, Violanti et al. 2013) from 6.46 Ma up to the Messinian
780 Salinity Crisis onset at 5.97 Ma. As previously observed in other pre-MSC successions,
781 the onset of the crisis is approximated by: 1) the last recovery of planktonic and benthic
782 foraminifera (Manzi et al. 2007, Manzi et al. 2011, Violanti et al. 2013), 2) the peaks of *U.*
783 *rotula* and *H. carteri* (Lozar et al. 2010, Violanti et al. 2013) and 3) an increase of the fresh
784 water input (based on $^{87}Sr/^{86}Sr$ values; Flecker et al. 2002, Roveri et al. 2014). These
785 events are recorded within an interval characterized by microbialitic and clastic carbonates
786 (included in the “barre jaune” of Orszag-Sperber et al. 2009), a few meters below the
787 clastic evaporites of the Kalavasos fm. (Manzi et al. 2016). This supports the interpretation
788 that the evaporites of Tokhni do not represent the MSC beginning (Manzi et al. 2016), but
789 instead the Stage 2 of Roveri et al. (2009), deposited after 5.60 Ma above the Messinian
790 Erosional Surface.
791 The estimated paleodepth reconstructed for the Psematismenos basin is upper bathyal
792 and did not significantly change from ca. 6.5 Ma up to the MSC onset. Remarkable
793 paleoceanographic changes are documented at ca. 6.4 and 6.1 Ma, coeval to the
794 uppermost major steps of the pre-MSC phase, and interpreted as increasingly stressed
795 surface and bottom water conditions (Blanc-Valleron et al. 2002, Sierro et al. 2003,
796 Kouwenhoven et al. 2006). It is hypothesized that from 6.4 Ma the increased runoff
797 favoured the stratification of the water column and enhanced nutrients levels in bottom and
798 surface waters at times of insolation maxima. Compared to the Western Mediterranean,
799 we observe a less severe oxygen reduction at the sea floor during insolation maxima,
800 probably caused by the episodic formation of intermediate/deep waters. During insolation
801 minima, excess evaporation in surface waters stimulated a vigorous mixing and we
802 speculate that the absence of benthic and planktonic foraminifera was due to the elevated

803 salinity. This indicates more extreme stressed conditions than in the Sorbas basin, where
804 planktonic foraminifera solely are generally reduced in abundance (Sierro et al. 2003).
805 After the deposition of the conglomerate at ca. 6.1 Ma, possibly related to a tectonic pulse,
806 micropaleontologic assemblages were reduced in abundance and diversity in response to
807 enhanced riverine influence. However, we note that a detectable decrease of the
808 connection with the global ocean can be argued based on the reduction of the $^{87}Sr/^{86}Sr$
809 values at the MSC onset.
810
811 7. Acknowledgements
812 This research was funded by a MIUR (Ministero dell'Istruzione, dell'Università e della
813 Ricerca, Italy) grant to M. Roveri (PRIN 2008). G. Gianelli and E.M. Selmo of the Physical
814 and Earth Science Department of the University of Parma are thanked for processing the
815 foraminifer samples and the O and C isotopic analysis, respectively. Iannis Panayides and
816 Zomenia Zomeni of the Geological Survey of the Republic of Cyprus are acknowledged for
817 their logistic support. A special thank is reserved to our colleagues Silvia Iaccarino, Maciej
818 Babel and Andrea Irace during the field trips in Cyprus. We are also grateful to an
819 anonymous reviewer for the appreciated suggestions. This is ISMAR-CNR, Bologna,
820 scientific contribution n. 1906.
821
822 8. References
823 Aubry, M.P., 1992. Late paleogene calcareous nannoplankton evolution: a tale of climatic
824 deterioration. In: Prothero, D.R., Berggren, W.A. (Eds.), Eocene–Oligocene Climatic and
825 Biotic Evolution. Princeton University Press, pp. 272– 309.
826
827 Ausin, B., Hernandez-Almeida, I., Flores, J.-A., Sierro, F.-J., Grosjean, M., Francés, G.,
828 Alonso, B. 2015. Development of coccolithophore-based transfer functions in the western

Mediterranean sea: a sea surface salinity reconstruction for the last 15.5 kyr. Climate of the Past 11, 1635-1651.

Bagnall, P.S., 1960. The geology and mineral resources of the Pano Lefkara-Larnaca area. Geological Survey Department Cyprus Memoir 5, 116 p.

Bartol, M., Pavšič, J., Dobnikar, M., Bernasconi, S., 2008. Unusual *Braarudosphaera bigelowii* and *Micrantholithus vesper* enrichment in the Early Miocene sediments from the Slovenian Corridor, a seaway linking the Central Paratethys and the Mediterranean. Palaeogeography, Palaeoclimatology, Palaeoecology 267, 77–88.

Baumann, K.-H., Saavedra-Pellitero, M., Böckel, B., Ott. C., 2016. Morphometry, biogeography and ecology of *Calcidiscus* and *Umbilicosphaera* in the South Atlantic. Revue de Micropaléontologie, in press.

Blanc-Valleron, M.M., Pierre, C., Caulet, J.P., Caruso, A., Rouchy, J.M., Cespuglio, G., Sprovieri, R., Pestrea, S., Di Stefano, E., 2002. Sedimentary, stable isotope and micropaleontological records of paleoceanographic change in the Messinian Tripoli Formation (Sicily, Italy). Palaeogeography, Palaeoclimatology, Palaeoecology 185, 255–286.

Boeckel, B., Baumann, K.-H., Henrich, R., Kinkel, H., 2006. Coccolith distribution patterns in South Atlantic and Southern Ocean surface sediments in relation to environmental gradients. Deep-Sea Research I 53, 1073–1099.

854 Boomer, I., Eisenhauer, G., 2002. Ostracod faunas as palaeoenvironmental indicators in
855 marginal marine environments. In: Holmes, J., Chivas, A. (Eds.), The Ostracoda:
856 Applications in Quaternary Research, Geophysical Monograph 131, 135–149.
857
858 Bown, P.R., 2005. Selective calcareous nannoplankton survivorship at the Cretaceous –
859 Tertiary boundary. Geology 33, 653–656.
860
861 Bown, P.R., Young, J.R., 1998. Techniques. In: Bown, P.R. (Ed.), Calcareous Nannofossil
862 Biostratigraphy. Kluwer Academic Publications, Dordrecht, Netherlands, pp. 16–28.
863
864 Bukry, D., 1974. Coccoliths as paleosalinity indicators-evidence from the Black Sea. In:
865 Degens, E.T., Ross, D.A. (Eds.), The Black Sea - Geology, chemistry, and biology:
866 American Association Petroleum Geologists Memoirs 2, pp. 353–363.
867
868 Cachão, M., Drago, T., Silva, A.D., Moita, T., Oliveira, A., Naughton, F., 2002. The secret
869 (estuarine?) life of *Helicosphaera carteri*: preliminary results. Journal of Nannoplankton
870 Research 24, 76–77.
871
872 Chadima, M., Hrouda, F., 2006. Remasoft 3.0 a user-friendly paleomagnetic data browser
873 and analyzer. Travaux Géophysiques XXVII, 20–21.
874
875 Dela Pierre, F., Bernardi, E., Cavagna, S., Clari, P., Gennari, R., Irace, A., Lozar, F., Lugli,
876 S., Manzi, V., Natalicchio, M., Roveri, M., Violanti, D., 2011. The record of the Messinian
877 salinity crisis in the Tertiary Piedmont Basin (NW Italy): the Alba section revisited.
878 Palaeogeography, Palaeoclimatology, Palaeoecology 310, 238–255.
879

880 Dittert, N., Baumann, K.H., Bickert, T., Henrich, R., Huber, R., Kinkel, H., Meggers, H.,
881 1999. Carbonate dissolution in the deep sea: methods, quantification and
882 paleoceanographic application. In: Fischer, G., Wefer, G. (Eds.), Use of Proxies in
883 Paleoceanography: Examples From the South Atlantic. Springer-Verlag, Berlin, pp. 255–
884 284.
885
886 Drinia, H., Antonarakou, A., Tsaparas, N., Kontakiotis, G., 2007. Palaeoenvironmental
887 conditions preceding the Messinian Salinity Crisis: a case study from Gavdos Island.
888 Geobios 40, 251–265.
889
890 Dudley, W.C., Nelson, C.S., 1989. Quaternary surface-water stable isotope signal from
891 calcareous nannofossils at DSDP Site 593, southern Tasman Sea. Marine
892 Micropaleontology 13 (4), 353 – 373.
893
894 Flecker, R., de Villiers, S., Ellam, R.M., 2002. Modelling the effect of evaporation on the
895 salinity–87Sr/86Sr relationship in modern and ancient marginal-marine systems: the
896 Mediterranean Messinian Salinity Crisis. Earth Planetary Science Letters 203, 221–233.
897
898 Flores, J.-A., Sierro, F.J., Filippelli, G.M., Bárcena, M.A., Pérez-Folgado, M., Vázquez, A.,
899 Utrilla, R., 2005. Surface water dynamics and phytoplankton communities during
900 deposition of cyclic late Messinian sapropels sequences in the western Mediterranean.
901 Marine Micropaleontology 56, 50–79.
902
903 Flores, J.A., Sierro, F.J., Francés, G., Vázquez, A., Zamarreno, I., 1997. The last 100,000
904 years in the western Mediterranean: sea surface water and frontal dynamics as revealed
905 by coccolithophores. Marine Micropaleontology 29, 351-366.

906

907 Flores, J.A., Sierro, F.J., Raffi, I., 1995. Evolution of the calcareous nannofossil
908 assemblage as a response to the paleoceanographic changes in the eastern equatorial
909 Pacific Ocean from 4 to 2 Ma (Leg 138, Sites 849 and 852). Proceedings of the ODP,
910 Scientific Results, vol. 138. Ocean Drilling Program, College Station, TX, pp. 163– 176.

911

912 Gass, T.M., 1960. The geology and mineral resources of the Dhali area. Geological
913 Survey Department Cyprus Memoir 4, 116 p.

914

915 Gennari, R., Manzi, V., Angeletti, A., Bertini, A., Biffi, U., Ceregato, A., Faranda, C., Gliozzi,
916 E., Lugli, S., Menichetti, E., Rosso, A., Roveri, M., Taviani, M., 2013. A shallow water
917 record of the onset of the Messinian salinity crisis in the Adriatic foredeep (Legnagnone
918 section, Northern Apennines). Palaeogeography, Palaeoclimatology, Palaeoecology 386,
919 145–164.

920

921 Gibbs, S., Shackleton, N., Young, J.R., 2004a. Orbitally forced climate signals in mid-
922 Pliocene nannofossil assemblages. Marine Micropaleontology 51, 39–56.

923

924 Gibbs, S., Shackleton, N., Young J. R., 2004b. Identification of dissolution patterns in
925 nannofossil assemblages: A high-resolution comparison of synchronous records from
926 Ceara rise, ODP Leg 154, Paleoceanography 19, PA1029.

927

928 Giraudeau, J., 1992. Distribution of recent nannofossils beneath the Benguela system:
929 southwest African continental margin. Marine Geology 108, 219-237.

930

931 Grothe, A., Sangiorgi, F., Mulders, Y.R., Vasiliev, I., Reichart, G.-J., Brinkhuis, H.,
932 Krijgsman, W., 2014. Black Sea desiccation during the Messinian Salinity Crisis: fact or
933 fiction? Geology 42, 563-566.
934
935 Hermoso, M., Horner, T.J., Minoletti, F., Rickaby, R.E.M., 2014. Constraints on the vital
936 effect in coccolithophore and dinoflagellate calcite by oxygen isotopic modification of
937 seawater. Geochimica et Cosmochimica Acta 141, 612-627.
938
939 Hilgen, F.J., Krijgsman, W., 1999. Cyclostratigraphy and astrochronology of the Tripoli
940 diatomite formation (pre-evaporite Messinian, Sicily, Italy). Terra Nova 11, 16–22.
941
942 Iaccarino, S.M., Premoli Silva, I., Biolzi, M., Foresi, L.M., Lirer, F., Turco, E., Petrizzo, M.R.
943 2007. Practical manual of Neogene Planktonic foraminifera. International School on
944 Planktonic Foraminifera. VI course: Neogene. Perugia.
945
946 Imai, R., Farida, M., Sato, T., Iryu, Y., 2015. Evidence for eutrophication in the
947 northwestern Pacific and eastern Indian oceans during the Miocene to Pleistocene based
948 on the nannofossil accumulation rate, *Discoaster* abundance, and coccolith size
949 distribution of Reticulofenestra. Marine Micropaleontology 116, 15–27.
950
951 Jorissen, F.J., 1987. The distribution of benthic foraminifera in the Adriatic Sea. Marine
952 Microplaeontology 12, 21–48.
953
954 Kaiho, K., 1994. Benthic foraminiferal dissolved-oxygen index and dissolved-oxygen levels
955 in the modern ocean Geology 22, 719–722.
956

957 Kameo, K., 2002. Late Pliocene Caribbean surface water dynamics and climatic changes
958 based on calcareous nannofossil records. Palaeogeography, Palaeoclimatology,
959 Palaeoecology 179, 211-226.
960
961 Kelly, D.C., Norris, R.D., Zachos, J.C., 2003. Deciphering the paleoceanographic
962 significance of Early Oligocene *Braarudosphaera* chalks in the South Atlantic. Marine
963 Micropaleontology 49, 49–63.
964
965 Kirschvink, J.L., 1980. The least-squares line and plane and the analysis of
966 palaeomagnetic data. Geophysical Journal of the Royal Astronomical Society 62, 699–718.
967
968 Kouwenhoven, T.J., Hilgen, F.J., van der Zwaan, G.J., 2003. Late Tortonian–early
969 Messinian stepwise disruption of the Mediterranean– Atlantic connections: constraints
970 from benthic foraminiferal and geochemical data. Palaeogeography, Palaeoclimatology,
971 Palaeoecology 198, 303–319.
972
973 Kouwenhoven, T.J., Morigi, C., Negri, A., Giunta, S., Krijgsman, W., Rouchy, J.-M., 2006.
974 Paleoenvironmental evolution of the eastern Mediterranean during the Messinian:
975 constraints from integrated microfossil data of the Pissouri Basin (Cyprus). Marine
976 Micropaleontology 60, 17–44.
977
978 Kouwenhoven, T.J., Seidenkrantz, M.-S., van der Zwaan, G.J., 1999. Deep-water
979 changes: the near-synchronous disappearance of a group of benthic foraminifera from the
980 late Miocene Mediterranean. Palaeogeography, Palaeoclimatology, Palaeoecology 152,
981 259–281.
982

983 Krhovsky, J., Adamova, J., Hladikova, J, Maslowska, H., 1992, Paleoenvironmental
984 changes across the Eocene/Oligocene boundary in the Zdanice and Pouzdrany units
985 (Western Carpathians, Czechoslovakia): the long-term trend and orbitally forced changes
986 in calcareous nannofossil assemblages. Proceeding IV INA Conference, Knihovnicka ZPN,
987 14 b, 2, p. 105 – 187.
988
989 Krijgsman,W., Blanc-Valleron, M.-M., Flecker, R., Hilgen, F.J., Kouwenhoven, T.J., Merle,
990 D., Orszag-Sperber, F., Rouchy, J.-M., 2002. The onset of the Messinian salinity crisis in
991 the Eastern Mediterranean Pissouri Basin, Cyprus. Earth and Planetary Science Letters
992 194, 299–310.
993
994 Krijgsman, W., Hilgen, F.J., Raffi, I., Sierro, F.J., Wilson, D.S., 1999a. Chronology, causes
995 and progression of the Mediterranean salinity crisis. Nature 400, 652–655.
996
997 Krijgsman, W., Langereis, C.G., Zachariasse, W.J., Boccaletti, M., Moratti, G., Gelati, R.,
998 Iaccarino, S., Papani, G., Villa, G., 1999b. Late Neogene evolution of the Taza–Guercif
999 Basin (Rifian Corridor, Morocco) and implications for the Messinian Salinity Crisis. Marine
1000 Geology 153, 147–160.
1001
1002 Krijgsman, W., Langereis, C.G., 2000. Magnetostratigraphy of the Zobzit and Koudiat
1003 Zarga sections (Taza–Guercif basin, Morocco): implications for the evolution of the Rifian
1004 Corridor. Marine and Petroleum Geology 17, 359–371.
1005
1006 Laskar, J., Robutel, P., Joutel, F., Gastineau,M., Correia, A., Levrard, B., 2004. A long-
1007 term numerical solution for the insolation quantities of the Earth. Astronomy and
1008 Astrophysics 428, 261–285.

1009

1010 Lozar, F., Violanti, D., Dela Pierre, F., Bernardi, E., Cavagna, S., Clari, P., Irace, A.,
1011 Martinetto, E., Trenkwalder, S., 2010. Calcareous nannofossils and foraminifers herald the
1012 Messinian Salinity Crisis: the Pollenzo section (Alba, Cuneo; NW Italy). Geobios 43, 21–32.

1013

1014 Lozar, F., Violanti, D., Bernardi, E., Dela Pierre, F., Natalicchio, M. Identifying the onset of
1015 the Messinian salinity crisis: a reassessment of the biochronostratigraphic tools (Piedmont
1016 Basin, NW Italy). This volume.

1017

1018 Manzi, V., Gennari, R., Hilgen, F., Krijgsman, W., Lugli, S., Roveri, M., Sierro, F.J., 2013.
1019 Age refinement of the Messinian salinity crisis onset in the Mediterranean. Terra Nova 25,
1020 315-322.

1021

1022 Manzi, V., Roveri, M., Gennari, R., Bertini, A., Biffi, U., Giunta, S., Iaccarino, S., Lanci, L.,
1023 Lugli, S., Negri, A., Riva, A., Rossi, M.E., Taviani, M., 2007. The deep-water counterpart of
1024 the Messinian Lower Evaporites in the Apennine foredeep: the Fanantello section
1025 (Northern Apennines, Italy). Palaeogeography, Palaeoclimatology, Palaeoecology 251,
1026 470–499.

1027

1028 Manzi, V., Lugli, S., Roveri, M., Dela Pierre, F., Gennari, R., Lozar, F., Natalicchio, M.,
1029 Schreiber, B.C., Taviani, M. Turco, E., 2016. The Messinian salinity crisis in Cyprus: a
1030 further step toward a new stratigraphic framework for Eastern Mediterranean. Basin
1031 Research 28, 207-236.

1032

1033 Manzi, V., Gennari, R., Lugli, S., Roveri, M., Schreiber, B.C., 2011. The Messinian
1034 “Calcare di Base” (Sicily, Italy) revisited. Geological Society of America Bulletin 123, 347–
1035 370.
1036
1037 McArthur, J.M., Howarth, R.J., Bailey, T.R., 2001. Strontium isotope stratigraphy:
1038 LOWESS version 3: best fit to the marine Sr-isotope curve for 0–509 Ma and
1039 accompanying look-up table for deriving numerical age. Journal of Geology 109, 155–170.
1040
1041 McIntyre, A., McIntyre, R., 1971. Coccolith concentrations and differential solution in
1042 oceanic sediments. In: Funnell, B.M., Riedel, W.R. (Eds.), The Micropaleontology of
1043 Oceans. Cambridge University Press, London, pp. 253– 261.
1044
1045 Murray, J.W., 2006. Ecology and Application of Benthic Foraminifera. Cambridge
1046 University Press. 426 pp.
1047
1048 Nijenhuis, I.A., Schenau, S.J., Van der Weijden, C.H., Hilgen, F.J., Lourens, L.J.,
1049 Zachariasse, W.J., 1996. On the origin of upper Miocene sapropelites: a case study from
1050 the Faneromeni section, Crete (Greece). Paleoceanography 11, 633–645.
1051
1052 Orszag-Sperber, F., Caruso, A., Blanc-Valleron, M.M., Merle, D., Rouchy, J.M., 2009. The
1053 onset of the Messinian salinity crisis: insights from Cyprus sections. Sedimentary Geology
1054 217, 52–64.
1055
1056 Pantazis, T.M., 1967. The geology and mineral resources of the Pharmakas – Kalavasos
1057 area. Geological Survey Department Cyprus Memoir 8, 190 p.
1058

1059 Peleo-Alampay, A.M., Mead, G.A., Wei, W., 1999. Unusual Oligocene *Braarudosphaera*-
1060 rich layers of the South Atlantic and their paleoceanographic implications. Journal of
1061 Nannoplankton Research 21, 17-26.
1062
1063 Perch-Nielsen, K., 1985. Cenozoic calcareous nannofossils. In: Bolli, H.M., Saunders, J.B.,
1064 Perch-Nielsen, K. (Eds.), Plankton Stratigraphy. Cambridge University Press, Cambridge,
1065 pp. 427–554.
1066
1067 Pérez-Folgado, M., Sierro, F.J., Barcena, M.A., Flores, J.A., Vazquez, A., Utrilla, R.,
1068 Hilgen, F.J., Krijgsman, W., Filippelli, G.M., 2003. Western versus eastern Mediterranean
1069 paleoceanographic response to astronomical forcing: a high-resolution microplankton
1070 study of precession-controlled sedimentary cycles during the Messinian. Palaeogeography,
1071 Palaeoclimatology, Palaeoecology 190, 317–334.
1072
1073 Pestrea, S., Blanc-Valleron, M.M., Rouchy, J.M., 2002. Les assemblages de diatomées
1074 des niveaux infra-gypseux du Messinien de Méditerranée (Espagne, Sicile Chypre).
1075 Geodiversitas 24, 543–583.
1076
1077 Raffi, I., Mozzato, C., Fornaciari, E., Hilgen, F.J., Rio, D., 2003. Late Miocene calcareous
1078 nannofossil biostratigraphy and astrobiochronology for the Mediterranean region.
1079 Micropalaeontology 49, 1–26.
1080
1081 Renaud, S., Ziveri, P., Broerse, A.T.C., 2002. Geographical and seasonal differences in
1082 morphology and dynamics of the coccolithophore *Calcidiscus leptoporus*. Marine
1083 Micropaleontology 46, 363–385.
1084

1085 Robertson, A.H.F., Eaton, S., Follows, E.J., Payne, A.S., 1995. Depositional processes
1086 and basin analysis of Messinian evaporites in Cyprus. Terra Nova 7, 233–253.
1087
1088 Rohling, E.J., Marino, G., and Grant, K.M., 2015. Mediterranean climate and
1089 oceanography and the periodic development of anoxic events (sapropels). Earth-Science
1090 Reviews 143, 62-97.
1091
1092 Roveri, M., Gennari, R., Lugli, S., Manzi, V., 2009. The terminal carbonate complex: the
1093 record of sea-level changes during the Messinian salinity crisis. GeoActa 8, 57–71.
1094
1095 Roveri, M., Lugli, S., Manzi, V., Gennari, R., Schreiber, B.C., 2014. High-resolution
1096 strontium isotope stratigraphy of the Messinian deep Mediterranean basins: implications
1097 for marginal to central basin correlation. Marine Geology 349, 113–125.
1098
1099 Sierro, F.J., Flores, J.A., Francés, G., Vazquez, A., Utrilla, R., Zamarreño, I., Erlenkeuser,
1100 H., Barcena, M.A., 2003. Orbitally-controlled oscillations in planktic communities and cyclic
1101 changes in western Mediterranean hydrography during the Messinian. Palaeogeography,
1102 Palaeoclimatology, Palaeoecology 190, 289–316.
1103
1104 Sierro, F.J., Hilgen, F.J., Krijgsman, W., Flores, J.A., 2001. The Abad composite (SE
1105 Spain): A Mediterranean reference section for the Mediterranean and the APTS.
1106 Palaeogeography, Palaeoclimatology, Palaeoecology 168, 141-169.
1107
1108 Stoll, H.M., Shimizu, N., Archer, D., Ziveri, P., 2007. Coccolithophore productivity response
1109 to greenhouse event of the Paleocene–Eocene thermal maximum. Earth Planetary
1110 Science Letters 258, 192–206.

Triantaphyllou, M.V., Tsaparas, N., Stamatakis, M., Dermitzakis, M.D., 1999. Calcareous nannofossil biostratigraphy and petrological analysis of the preevaporitic diatomaceous sediments from Gavdos Island, southern Greece. Neues Jahrbuch für Geologie und Pälontologie Monatshefte 161–178.

Van der Zwaan, G.J., 1982. Paleoecology of late Miocene Mediterranean foraminifera. Utrecht Micropaleontological Bulletin 25, 201 p.

Vasiliev, I., Reichart, G.-J, Grothe, A., Sinninghe Damsté, J.P., Krijgsman, W., Sangiorgi, F., Weijer, J.W.H., van Roij, L., 2015. Recurrent phases of drought in the upper Miocene of the Black Sea region. Palaeogeography, Palaeoclimatology, Palaeoecology 423, 18–31.

Violanti D., Lozar F., Natalicchio M., Dela Pierre F., Bernardi E., Clari P., Cavagna S., 2013. Microfossili tolleranti condizioni di stress ambientale del Messiniano pre-evaporitico di Pollenzo (Piemonte, Italia nord- occidentale). Bollettino della Società Paleontologica Italiana 52, 45-54.

Wade, B.S., Bown, P.R., 2006. Calcareous nannofossils in extreme environment: the Messinian Salinity Crisis, Polemi Basin, Cyprus. Palaeogeography Palaeoclimatology Palaeoecology 233, 271–286.

Zijderveld, J.D.A., 1967. A. C. demagnetization of rocks: Analysis of results. In: Collinson, D.W., Creer, K.M., Runcorn, S.K. (Eds.), Methods in paleomagnetism. Elsevier, New York, 254–256 p.

1137 Ziveri, P., Baumann, K.-H., Böckel, B., Bollmann, J., Young, J.R., 2004. Present day
1138 coccolithophore biogeography of the Atlantic Ocean. In: Thierstein, H.R., Young, J.R.
1139 (Eds.), Coccolithophores: From Molecular Processes to Global Impact. Springer Verlag, pp.
1140 529–562.
1141
1142 Ziveri, P., de Bernardi, B., Baumann, K.-H., Stoll, H.M., Mortyn, P.G., 2007. Sinking of
1143 coccolith carbonate and potential contribution to organic carbon ballasting in the deep
1144 ocean. Deep Sea Research Part II. Topical Studies in Oceanography 54 (5–7), 659–675.
1145
1146 Ziveri, P., Stoll, H., Probert, I., Klaas, C., Geisen, M., Ganssen, G., Young, J., 2003. Stable
1147 'vital effects' in coccolith calcite. Earth and Planetary Science Letters 210, 137-149.

1148 Figure captions

1149 Fig. 1 - A) Generalized geological map of the central and eastern Mediterranean and B) of
1150 the south-western portion of the Cyprus Island with the indication of the position of the
1151 Tokhni (Orszag-Sperber et al. 2009, Manzi et al. 2016, this study) and Pissouri (Krijgsman
1152 et al. 2002, Kouwenohven et al. 2006) sections.

1153

1154 Fig. 2 - Lithological log of the four sub-sections outcropping near the Tokhni village. The
1155 dip and the inclination of the strata in the Pakhna and Kalavasos Formations are shown in
1156 order to highlight the presence of an unconformity related to the Messinian Erosional
1157 Surface (MES). The base of the Tokhni composite section (BTCS) is indicated with an
1158 arrow in sub-section To-1. The black bar next to sub-sections To-1, 2 and 3 shows the
1159 interval sampled for the quantitative calcareous nannofossil analysis and semi-quantitative
1160 foraminifer analysis.

1161

1162 Fig. 3 - Magnetostratigraphy of sub-section To-1. A) Plots of the inclination and declination
1163 of the characteristic remanent magnetization (ChRM). B) Stereoplot of the tilt corrected
1164 ChRM directions; the relative statistical values are reported for the normal and reverse
1165 samples in the upper and lower box, respectively. C) Stereoplots, Zijderveld and
1166 demagnetization (M/M_{max}) diagrams relative to the thermal demagnetization paths for three
1167 selected samples.

1168

1169 Fig. 4 - Plots of the abundance (n° of specimens/field) of the planktonic and benthic
1170 foraminifer taxa considered in this study, total abundance of planktonic and benthic
1171 foraminifera (black and grey line respectively) and P/B ratio (%). The abundances of
1172 sinistrally and dextrally coiled *N. acostaensis* are plotted with increasing values from left to
1173 right (black line) at the bottom of the plot and from right to left (grey line) at the top of the

1174 plot, respectively. The asterisks indicate samples not considered for semi-quantitative
1175 analyses.
1176
1177 Fig. 5 - Plots of the total abundance of calcareous nannofossil (n/mm^2) and relative
1178 abundances (%) of the taxa considered in this study. Note that *B. bigelowii* is only plotted
1179 as n/mm^2 and the *D. variabilis* gr. is plotted as n/mm^2 and % because of their scattered
1180 occurrences along the section.
1181
1182 Fig. 6 - Plots of the bulk Oxygen and Carbon isotopic values (both measured in shales and
1183 limestones) and of the bulk Sr isotopic ratio (only measured in limestones) of the Tokhni
1184 composite section.
1185
1186 Fig. 7 - Biomagnetostratigraphic and cyclostratigraphic correlation of the Tokhni composite
1187 section to the Pollenzo (Lozar et al. 2010, Violanti et al. 2013), Perales (modified after
1188 Sierro et al. 2001 and Manzi et al. 2013) and Falconara (modified after Hilgen and
1189 Krijgsman 1999, Blanc-Valleron et al. 2002 and Manzi et al. 2011) sections. The
1190 successions are tuned to the 65°N summer insolation curve (Laskar et al. 2004).
1191 Planktonic foraminifer events are indicated by numbers following the codification of Sierro
1192 et al. (2001) (a letter is added for new bioevents): 12) first occurrence (FO) of *T. multiloba*;
1193 13) Last regular influx (Lri) of *N. acostaensis* sinistral coiling; 14) first abundant occurrence
1194 (FAO) of *N. acostaensis* dextral coiling; 15) 1st influx of *G. scitula*; 15a) abundance influx of
1195 *T. multiloba*; 16) 1st influx of *N. acostaensis* sinistral coiling; 17) 2nd influx of *G. scitula*; 18)
1196 2nd influx of *N. acostaensis* sinistral coiling; 18a) last occurrence (LO) of *T. multiloba*; 19p)
1197 last recovery (LR) of planktonic foraminifera ; 19b) last recovery (LR) of benthic
1198 foraminifera. Calcareous nannofossil events (Violanti et al., 2013): a) *H. carteri* peak; b) *U.*
1199 *rotula* peak. On the left side of the figure, the boundaries between the pre-MSC stage,

1200 stage 1 and 2 of Roveri et al. (2009) and the MSC chronology are indicated. Note that a
1201 hiatus of ca. 350 kyr is present between stage 1 and 2 due to the erosion associated with
1202 the Messinian erosional surface (MES).
1203
1204 Fig. 8 - Summary of the paleoenvironmental changes recognized in the Tokhni composite
1205 section. The paleoenvironmental interpretation of the chronologically unconstrained
1206 lowermost 11 m of the section relies upon qualitative observations on foraminifera. The
1207 black star beside the insolation curve indicates the position of the influx of *B. bigelowii*,
1208 suggesting a transient connection with the paleo-Black sea. On the right side of the figure,
1209 the boundaries between the pre-MSC stage, stage 1 and 2 of Roveri et al. (2009) and the
1210 MSC chronology are indicated. Note that a hiatus of ca. 350 kyr is present between stage
1211 1 and 2 due to the erosion associated with the Messinian erosional surface (MES).

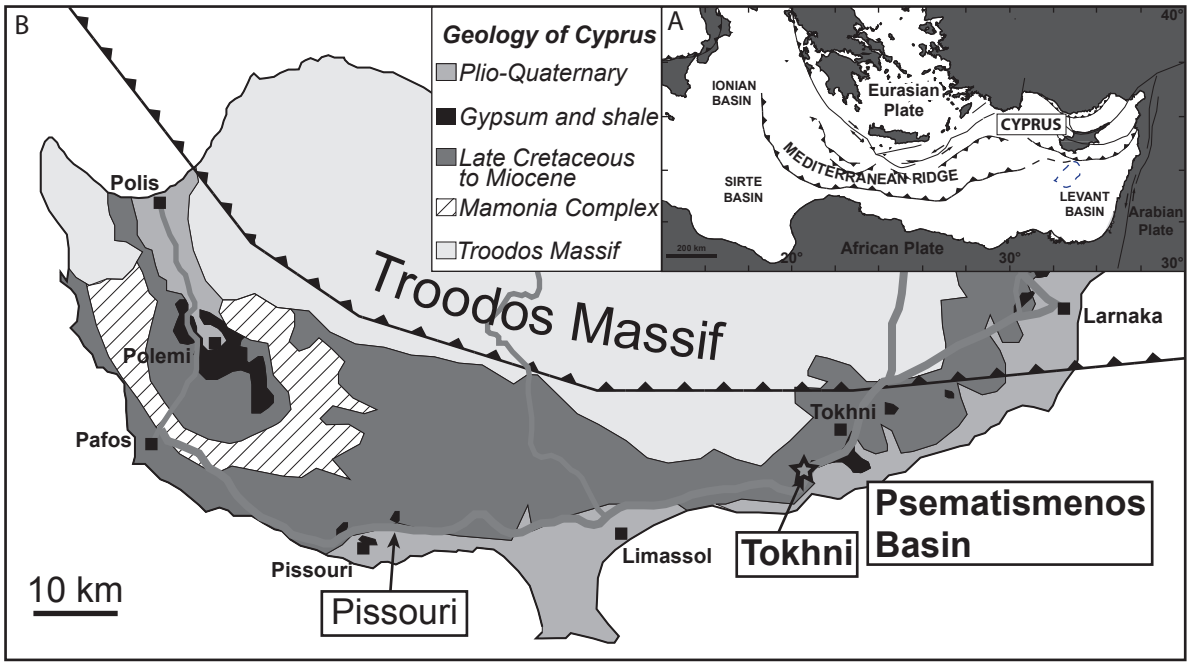
B
Geology of Cyprus
Plio-Quaternary
Gypsum and shale
Late Cretaceous to Miocene
Mamonia Complex
Troodos Massif
A
IONIAN BASIN
Eurasian Plate
CYPRUS
MEDITERRANEAN RIDGE
SIRTE BASIN
LEVANT BASIN
Arabian Plate
African Plate
200 km
20°
30°
40°
Polis
Troodos Massif
Larnaka
Polemi
Tokhni
Pafos
Psematismenos Basin
Limassol
Tokhni
Pissouri
Pissouri
10 km

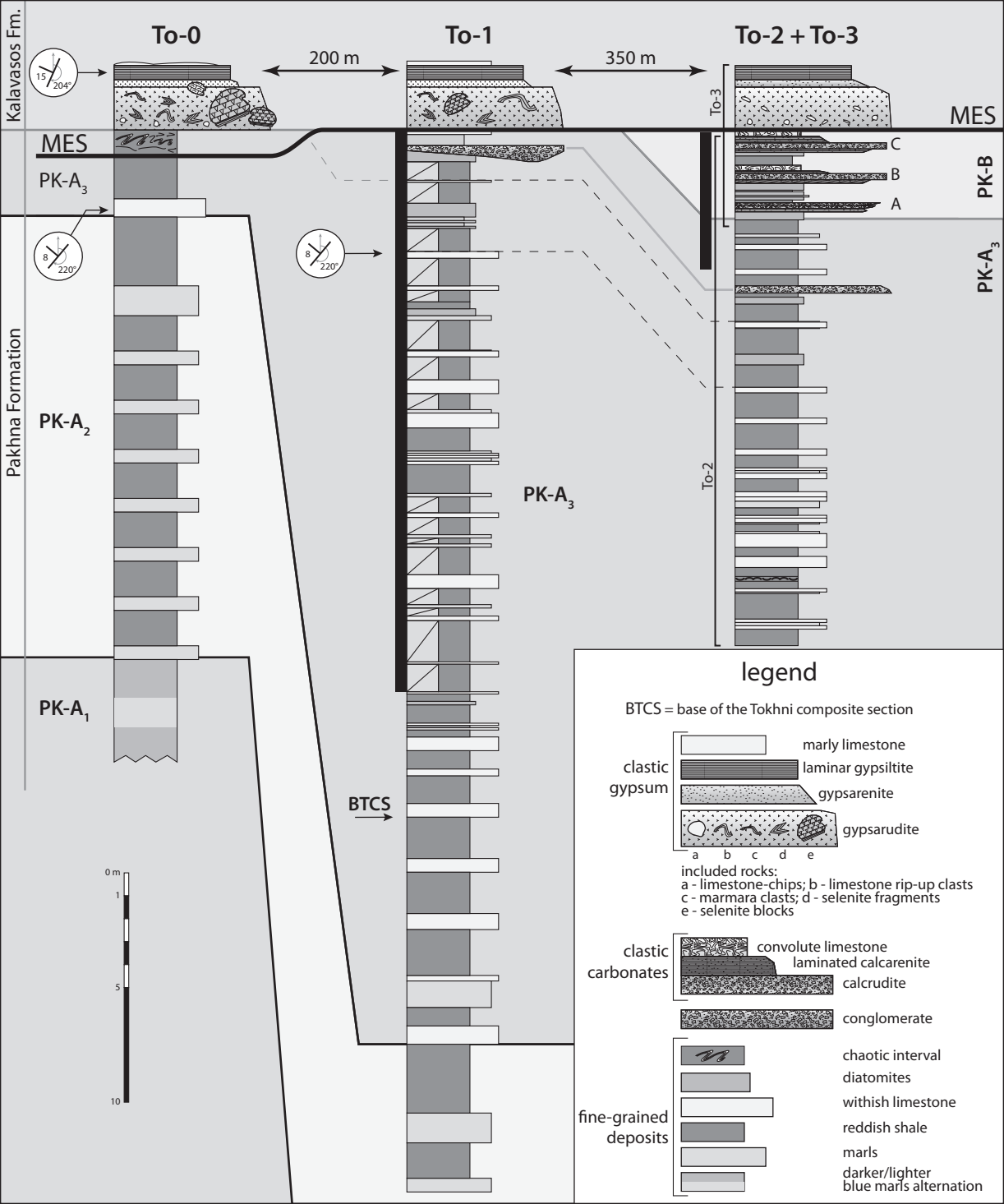
To-0
To-1
To-2 + To-3
200 m
350 m
Kalavasos Fm.
Pakhna Formation
MES
PK-A3
PK-A2
PK-A1
PK-B
C
B
A
To-3
To-2
BTCS
0 m
1
5
10
15
204°
8
220°
legend
BTCS = base of the Tokhni composite section
clastic gypsum
marly limestone
laminar gypsiltite
gypsarenite
gypsarudite
a b c d e
included rocks:
a - limestone-chips; b - limestone rip-up clasts
c - marmara clasts; d - selenite fragments
e - selenite blocks
clastic carbonates
convolute limestone
laminated calcarenite
calcrudite
conglomerate
fine-grained deposits
chaotic interval
diatomites
withish limestone
reddish shale
marls
darker/lighter blue marls alternation

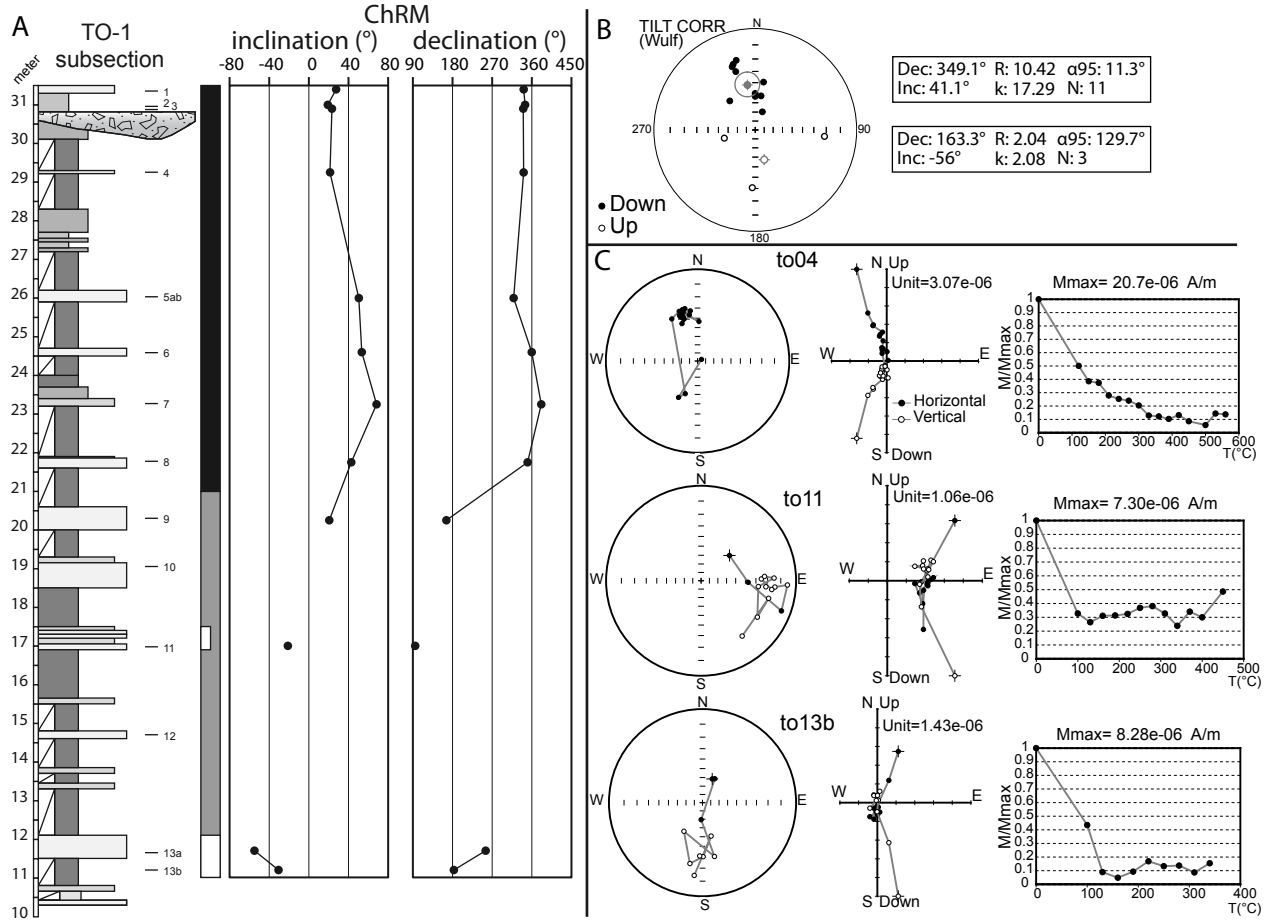
A
TO-1
subsection
meter
ChRM
inclination (°)
declination (°)
-80 -40 0 40 80 90 180 270 360 450
1
2 3
4
5ab
6
7
8
9
10
11
12
13a
13b
B
TILT CORR
(Wulf)
N
270
90
180
Dec: 349.1° R: 10.42 α95: 11.3°
Inc: 41.1° k: 17.29 N: 11
Dec: 163.3° R: 2.04 α95: 129.7°
Inc: -56° k: 2.08 N: 3
• Down
◦ Up
C
to04
N Up
Unit=3.07e-06
Horizontal
Vertical
S Down
Mmax= 20.7e-06 A/m
M/Mmax
T(°C)
to11
Unit=1.06e-06
Mmax= 7.30e-06 A/m
to13b
Unit=1.43e-06
Mmax= 8.28e-06 A/m

Figure 3

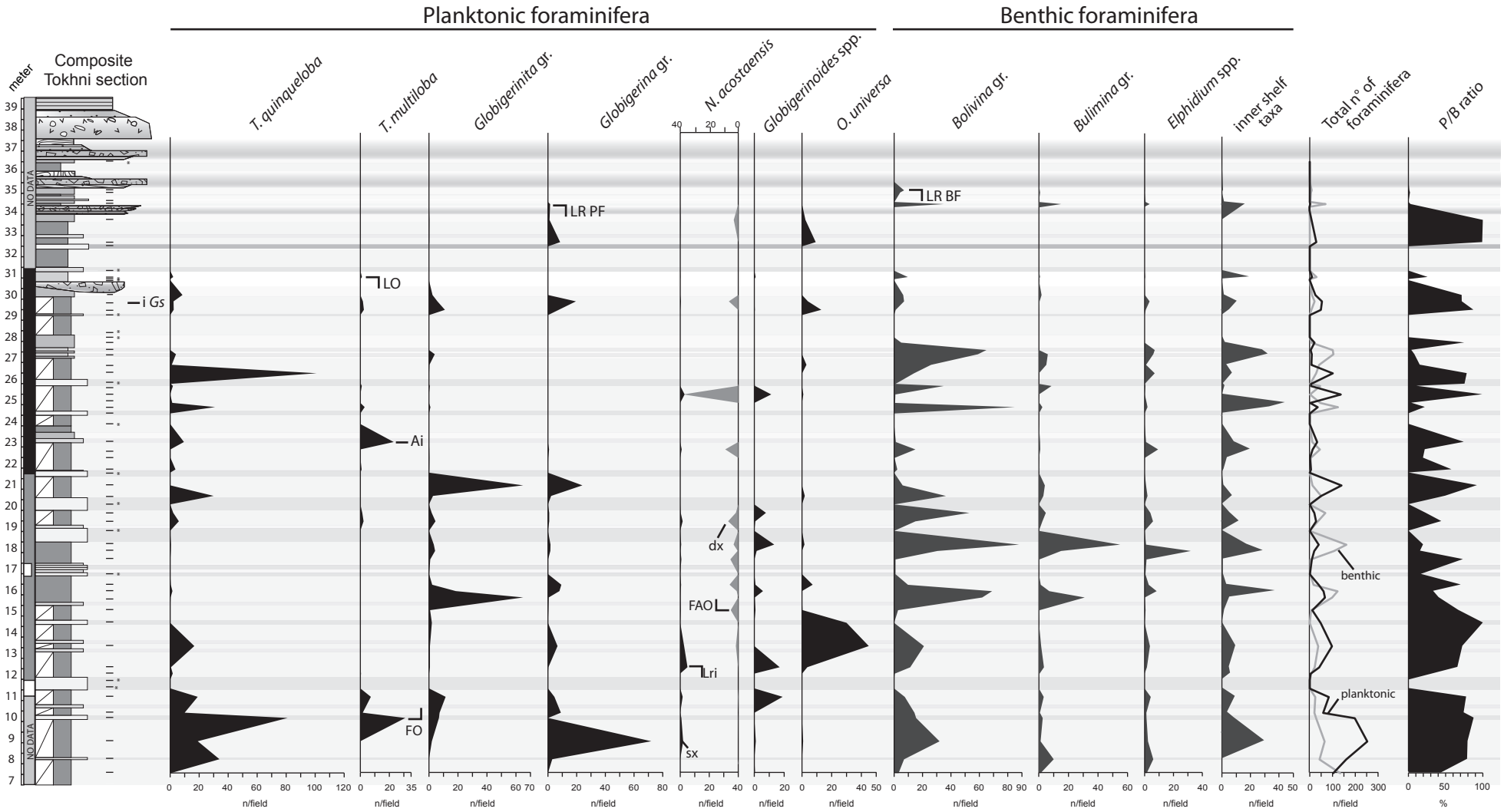
Planktonic foraminifera
Benthic foraminifera
meter
Composite Tokhni section
NO DATA
NO DATA
i Gs
LO
Ai
FO
LR PF
LR BF
dx
sx
FAO
Lri
benthic
planktonic
T. quinqueloba
T. multiloba
Globigerinita gr.
Globigerina gr.
N. acostaensis
Globigerinoides spp.
O. universa
Bolivina gr.
Bulimina gr.
Elphidium spp.
inner shelf taxa
Total n° of foraminifera
P/B ratio
n/field
%

Figure 4

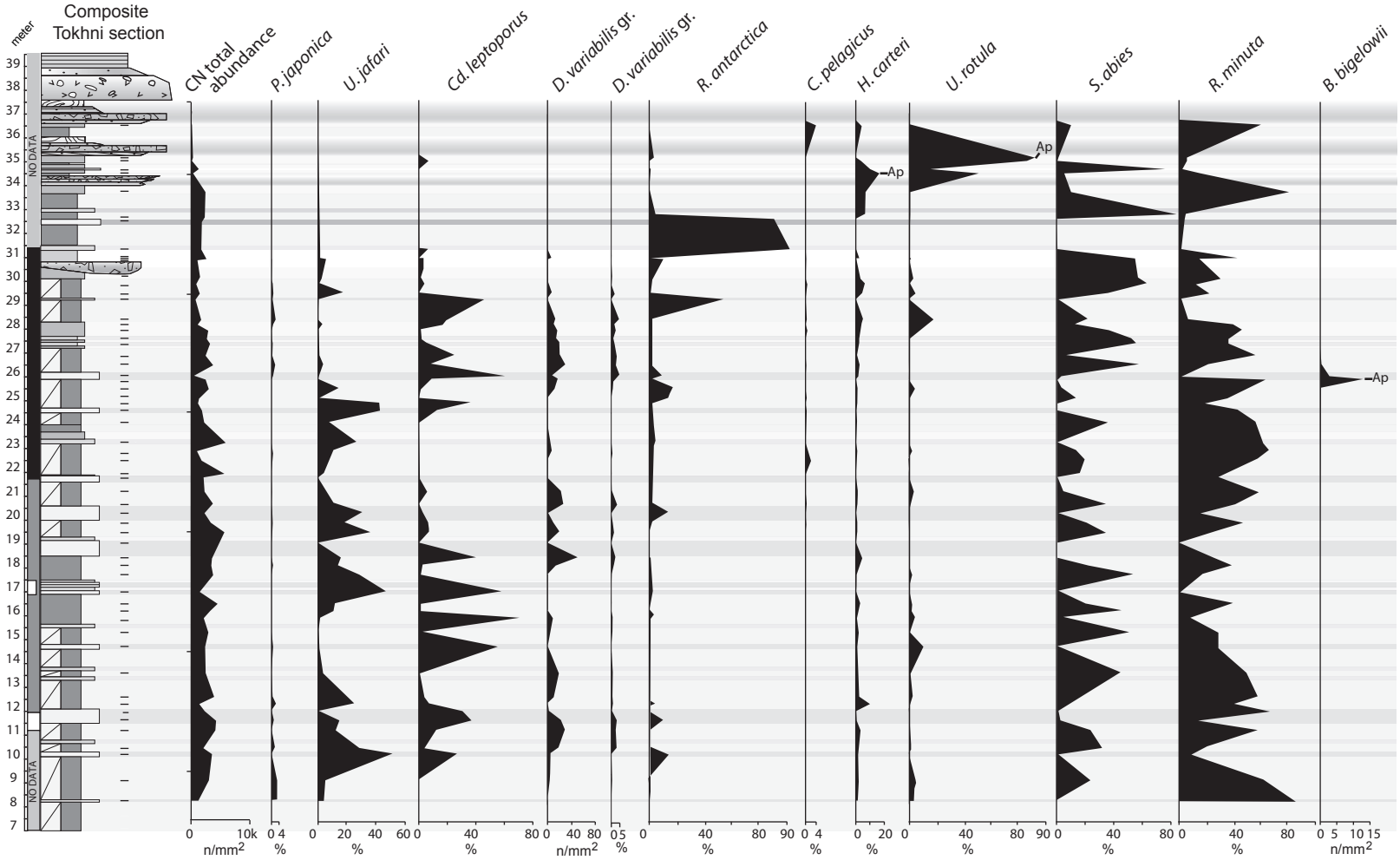
Composite
Tokhni section
meter
NO DATA
NO DATA
CN total abundance
P. japonica
U. jafari
Cd. leptoporus
D. variabilis gr.
D. variabilis gr.
R. antarctica
C. pelagicus
H. carteri
U. rotula
S. abies
R. minuta
B. bigelowii
Ap
Ap
Ap
n/mm2
%
%
%
n/mm2
%
%
%
%
%
%
%
n/mm2

Figure 5

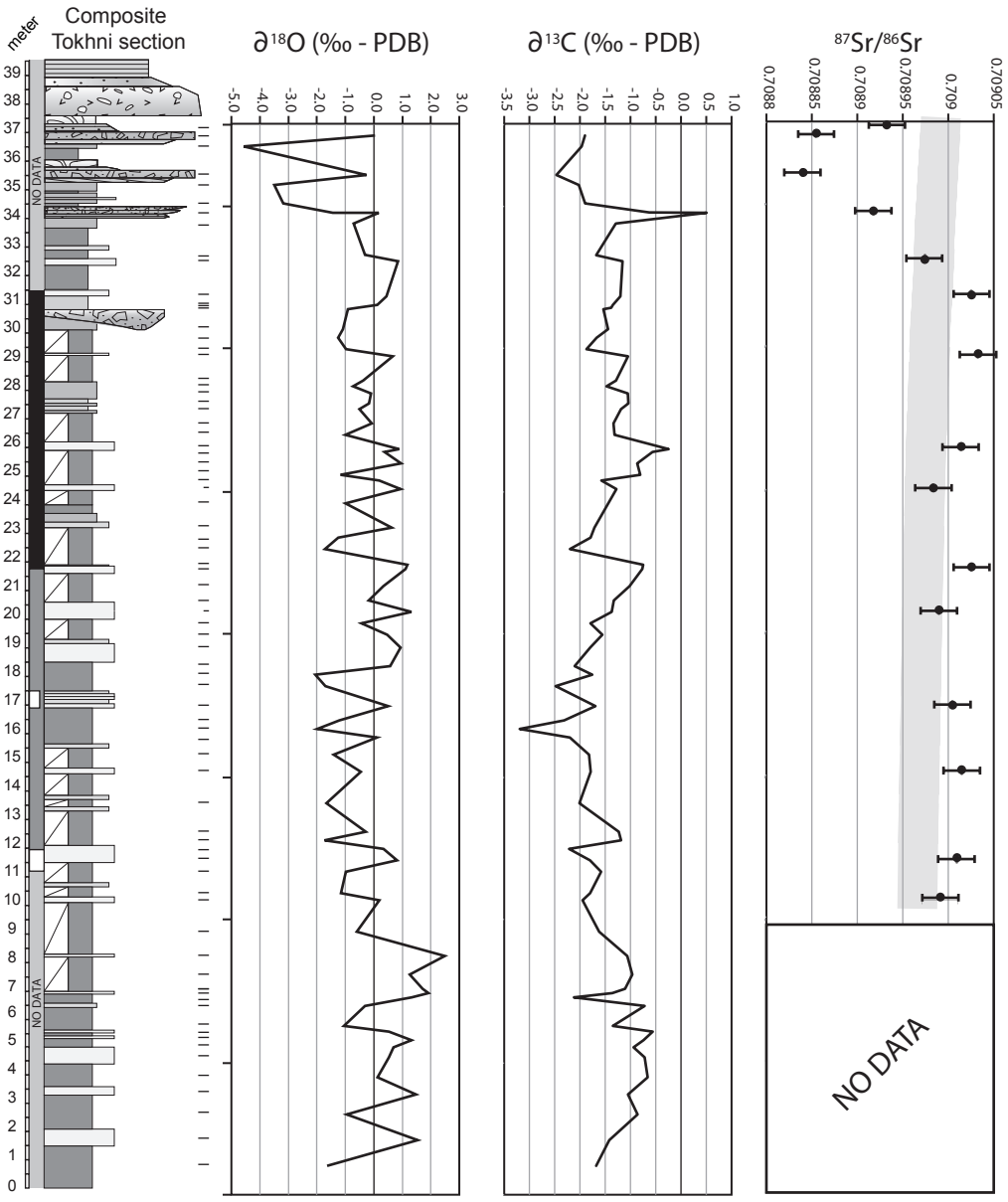
meter
Composite
Tokhni section
NO DATA
NO DATA
∂18O (‰ - PDB)
-5.0
-4.0
-3.0
-2.0
-1.0
0.0
1.0
2.0
3.0
∂13C (‰ - PDB)
-3.5
-3.0
-2.5
-2.0
-1.5
-1.0
-0.5
0.0
0.5
1.0
87Sr/86Sr
0.7088
0.70885
0.7089
0.70895
0.709
0.70905
NO DATA

Figure 6

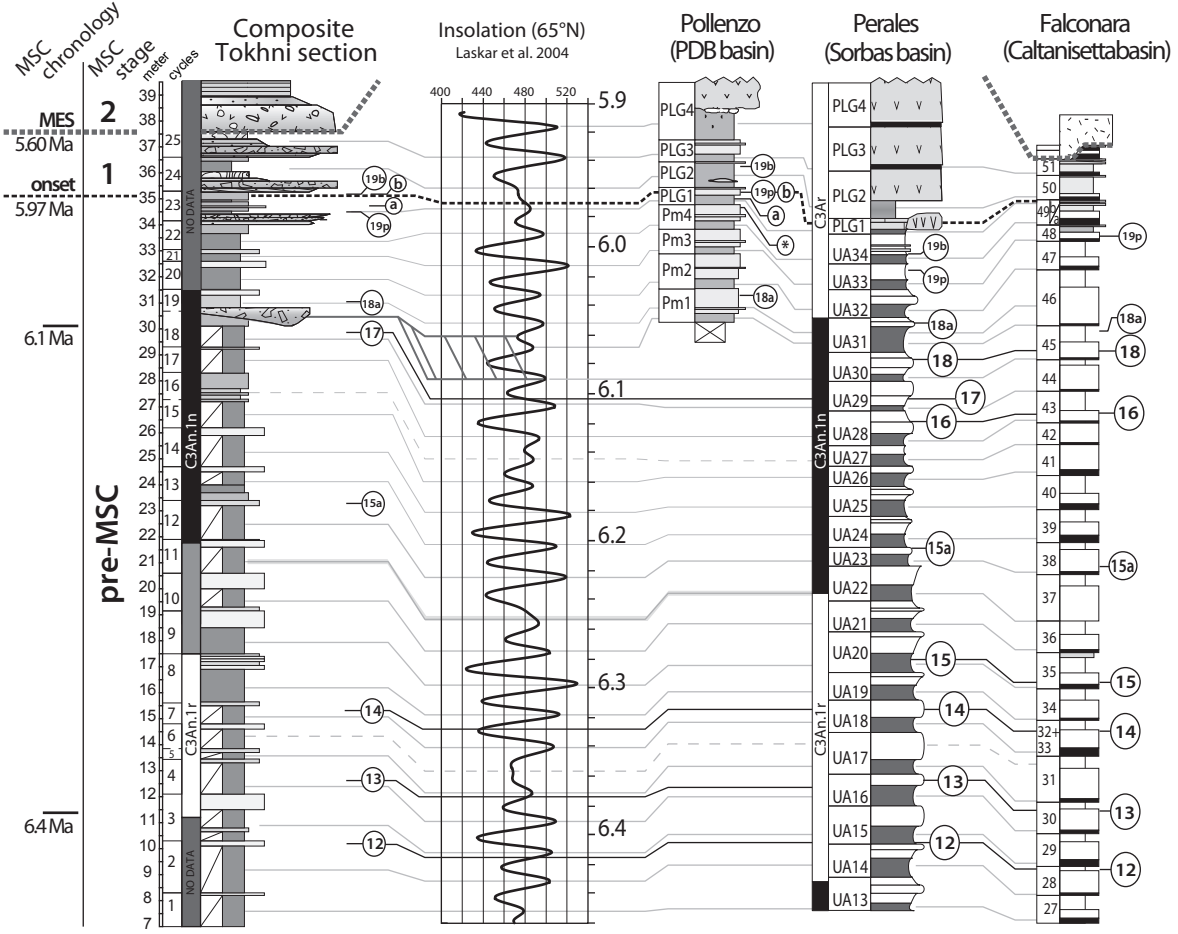
MSC chronology
MSC stage
meter
cycles
Composite Tokhni section
Insolation (65°N)
Laskar et al. 2004
Pollenzo (PDB basin)
Perales (Sorbas basin)
Falconara (Caltanisettabasin)
MES
5.60 Ma
onset
5.97 Ma
6.1 Ma
6.4 Ma
pre-MSC
NO DATA
C3An.1n
C3An.1r
C3Ar
PLG4
PLG3
PLG2
PLG1
Pm4
Pm3
Pm2
Pm1
UA34
UA33
UA32
UA31
UA30
UA29
UA28
UA27
UA26
UA25
UA24
UA23
UA22
UA21
UA20
UA19
UA18
UA17
UA16
UA15
UA14
UA13

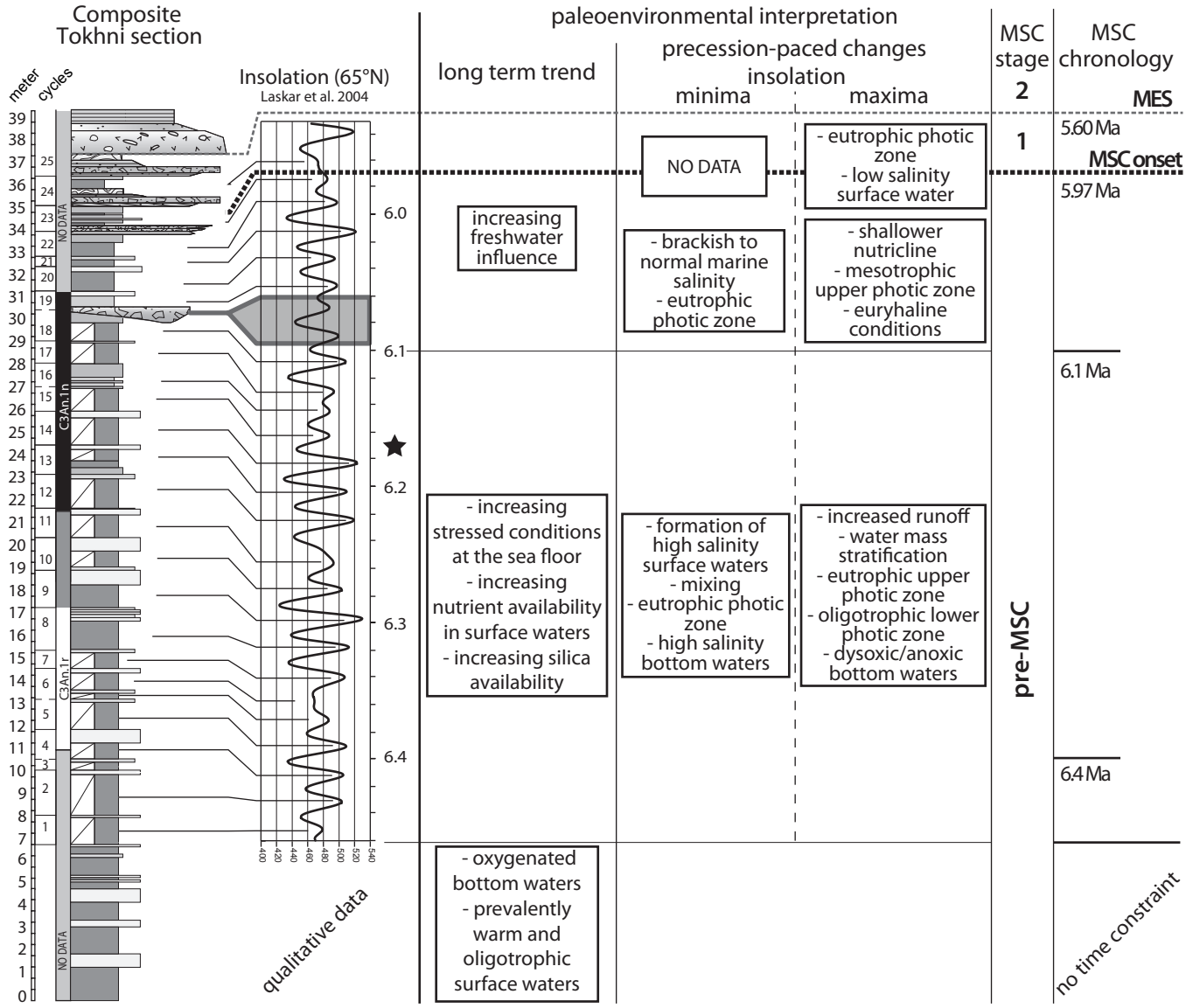
Composite Tokhni section
meter
cycles
Insolation (65°N)
Laskar et al. 2004
NO DATA
C3An.1n
C3An.1r
NO DATA
qualitative data
paleoenvironmental interpretation
long term trend
precession-paced changes
insolation
minima
maxima
MSC stage
MSC chronology
MES
5.60 Ma
MSC onset
5.97 Ma
6.1 Ma
6.4 Ma
no time constraint
pre-MSC
2
1
increasing freshwater influence
NO DATA
- eutrophic photic zone
- low salinity surface water
- brackish to normal marine salinity
- eutrophic photic zone
- shallower nutricline
- mesotrophic upper photic zone
- euryhaline conditions
- increasing stressed conditions at the sea floor
- increasing nutrient availability in surface waters
- increasing silica availability
- formation of high salinity surface waters
- mixing
- eutrophic photic zone
- high salinity bottom waters
- increased runoff
- water mass stratification
- eutrophic upper photic zone
- oligotrophic lower photic zone
- dysoxic/anoxic bottom waters
- oxygenated bottom waters
- prevalently warm and oligotrophic surface waters

Figure 8